

Elastic constants and ultrasonic attenuation in the cone state of the frustrated antiferromagnet Cs_2CuCl_4

Andreas Kreisel and Peter Kopietz
*Institut für Theoretische Physik, Universität Frankfurt,
Max-von-Laue Strasse 1, 60438 Frankfurt, Germany*

Pham Thanh Cong, Bernd Wolf, and Michael Lang
Physikalisches Institut, Universität Frankfurt, Max-von-Laue Strasse 1, 60438 Frankfurt, Germany
(Dated: July 15, 2011)

In an external magnetic field perpendicular to the plane of the layers, the quasi two-dimensional frustrated antiferromagnet Cs_2CuCl_4 exhibits a magnetically ordered “cone state” at low temperatures. In this state the component of the magnetic moments in field direction is finite, while their projection onto the plane of the layers forms a spiral. We present both theoretical and experimental results for the magnetic-field dependence of the elastic constants and the ultrasonic attenuation rate in the cone state. Our theoretical analysis is based on the usual spin-wave expansion around the classical ground state of a Heisenberg model on an anisotropic triangular lattice with Dzyaloshinskii–Moriya interactions. Magnon-phonon interactions are modeled by expanding the exchange interactions up to second order in powers of the phonon coordinates. As long as the external magnetic field is not too close to the critical field where the cone state becomes unstable, we obtain reasonable agreement between theory and experiment, suggesting that at least in this regime magnons behave as well-defined quasiparticles. We also show that the assumption of well-defined magnons implies that at long wavelengths the ultrasonic attenuation rate in the cone state of Cs_2CuCl_4 is proportional to the fourth power of the phonon momentum.

PACS numbers: 43.35.+d, 75.10.Jm, 75.30.Ds, 72.55.+s

I. INTRODUCTION

In recent years a large amount of theoretical and experimental work has been devoted to low-dimensional quantum magnets on frustrated lattices.¹ In these systems enhanced quantum fluctuations and competing interactions can stabilize magnetically disordered ground states in certain parameter regimes. The phase transitions between ordered and disordered phases as a function of some nonthermal control parameter, such as an external magnetic field, have attracted a lot of attention. An important realization of such a frustrated magnet exhibiting a rather complex phase diagram, including magnetically ordered and disordered phases, is the magnetic insulator Cs_2CuCl_4 . This material was synthesized and characterized about 15 years ago.^{2,3} Coldea *et al.*⁴ determined the magnetic structure and pointed out that it is a realization of a triangular lattice antiferromagnet with two different exchange couplings J and J' whose magnitude is less than 1 meV. The effective g -factor was obtained by electron spin resonance measurements⁵. Later on, an effective model Hamiltonian was deduced from high field measurements.⁶ The observation of Bose-Einstein condensation of magnons⁷ and investigations on the phase diagram followed. An ordered cone state and a ferromagnetic phase which are connected by a quantum critical point were discovered. The challenge to gain a quantitative microscopic understanding of the experimental observations has motivated a large number of recent theoretical works.^{8–17}

There are two complementary theoretical points of

view: On the one hand, it has been argued that the difference in the two competing exchange couplings in the layers is sufficiently large to view the system as a collection of weakly coupled spin chains.^{14–17} The properties of the decoupled one-dimensional spin chains can then be obtained nonperturbatively using bosonization techniques, while the weak coupling between the chains is usually included using some kind of mean-field approximation. Because in this approach one assumes that the elementary excitations of the system can be connected to the spinons of the one-dimensional spin chains, this approach is most natural to describe the spin-liquid sector of the phase diagram. On the other hand, for the description of the part of the phase diagram which exhibits magnetic order, it seems to be more natural to start from the usual spin-wave picture and expand in fluctuations around an ordered classical ground state using the Holstein–Primakoff transformation.^{8–12,18,19} Formally, this approach is based on the smallness of the inverse spin quantum number $1/S$. However, even for $S = 1/2$ the result of the $1/S$ -expansion has often been surprisingly accurate, at least for quantum antiferromagnets on nonfrustrated lattices. It is therefore reasonable to expect that the $1/S$ -expansion is a good starting point to describe the magnetically ordered cone state of Cs_2CuCl_4 , which is stable at sufficiently low temperatures and in a range of magnetic fields oriented perpendicular to the layers. It turns out, however, that the $1/S$ -expansion in the cone state has been only partially successful because experimentally observed large quantum renormalizations of the exchange energies could not be explained by including

only the leading $1/S$ corrections to linear spin-wave theory. In particular, Veillette *et al.*⁹ calculated the dynamical structure factor in the cone state of Cs_2CuCl_4 , including the leading $1/S$ corrections to linear spin-wave theory. Although they found that the spin-wave interactions explain, on a qualitative level, many experimentally observed features, there was no quantitative agreement between theory and experiment. Whether or not infinite resummations of the $1/S$ -expansion retaining certain types of interaction processes would improve the agreement with experiments remains an open problem.

The purpose of this paper is to further investigate the validity of the spin-wave picture in the cone state of Cs_2CuCl_4 . Therefore, we present both experimental and theoretical results for the magnetic-field dependence of the elastic constants and the ultrasonic attenuation rate in Cs_2CuCl_4 at low temperatures and in the range of magnetic fields where the cone state is stable. Since the lattice vibrations are coupled to the spin excitations, the magnetic-field dependence of the energy and the damping of the phonon excitations provides useful information about the magnetic excitations. Indeed, in the vicinity of a magnetic phase transition one expects rather strong magnetic-field dependence of the phonon degrees of freedom, so that one can map out the phase diagram by measuring the elastic constants and the phonon damping which determines the ultrasonic attenuation rate.²⁰

Previous ultrasonic investigations of the longitudinal c_{22} -mode on single crystals of Cs_2CuCl_4 by Sytcheva *et al.*²¹ focused on the nature of the different phases and on the field-induced quantum critical point. Our theoretical approach is complementary to the approach adopted by the authors of Ref. [21], who obtained the elastic constants from simple phenomenological expressions for the thermodynamic potentials²⁰ and relied on phenomenological relaxation rates to determine the ultrasonic attenuation rate.²¹ In contrast, our derivation of the ultrasonic attenuation rate and the elastic constants is based on a microscopic calculation starting from the relevant Heisenberg Hamiltonian. Although the theory of magnetoelastic interactions is well established^{20,22} there have been only a few previous investigations of the interplay between spins and lattice vibrations in triangular lattice antiferromagnets^{23–25} and other frustrated spin systems.²⁶ In particular, microscopic investigations of the interaction between spin and lattice degrees of freedom in the cone state of Cs_2CuCl_4 have so far not been carried out.

The rest of this paper is organized as follows: Our starting point in Sec. II A is the assumption that the interplay between magnetic and lattice degrees of freedom in Cs_2CuCl_4 can be described by a spin $S = 1/2$ quantum Heisenberg antiferromagnet on a distorted triangular lattice with Dzyaloshinskii–Moriya (DM) anisotropy in an external magnetic field. The coupling between magnons and phonons arises from the fact that the exchange integrals and the DM interactions depend on the distances between the actual positions of the ions, which

in turn depend on the phonon coordinates. Assuming an ordered classical ground state (the cone state discussed in Sec. II B), we model the low-lying spin excitations in terms of suitably defined interacting Holstein–Primakoff bosons. By expanding the exchange integrals to second order in the phonon coordinates we obtain in Sec. II C the effective magnon-phonon interaction. In particular, we explicitly derive the relevant interaction vertices, which exhibit rather complicated momentum dependencies due to the spiral spin structure of the cone state.

In Sec. III we then use functional integration techniques and diagrammatic perturbation theory to calculate the renormalization of the phonon energies due to the coupling to the magnons. Formally, this renormalization can be described in terms of a momentum- and frequency-dependent phonon self-energy, whose real part gives the shift in the phonon velocities (which are related to the elastic constants), and whose imaginary part gives the phonon damping (which is related to the ultrasonic attenuation rate). Using the fact that in Cs_2CuCl_4 the velocities of acoustic phonons are large compared with the magnon velocities, we can derive analytic expressions for the magnetic-field-dependent part of the elastic constants and the ultrasonic attenuation rate. In particular, we show that for small wavevectors \mathbf{k} the ultrasonic attenuation rate in Cs_2CuCl_4 is proportional to k^4 .

In Sec. IV we present our experimental results for the magnetic-field dependence of the elastic constants and the ultrasonic attenuation rate in the cone state of Cs_2CuCl_4 and compare them with our theoretical predictions. In the regime of magnetic fields where our perturbative calculation is valid we find good agreement between theory and experiment. Finally, in Sec. V we present our conclusions and discuss some open problems. In the appendix we evaluate the contribution of scattering processes involving intermediate states with one phonon and one magnon to the ultrasonic attenuation rate; we show that in Cs_2CuCl_4 the smallness of the magnon velocities in comparison with the phonon velocities guarantees that these processes are small compared with the processes considered in Sec. III B.

II. MAGNON-PHONON INTERACTIONS IN THE CONE STATE OF Cs_2CuCl_4

A. Spin-phonon Hamiltonian

To model the magnetoelastic properties of the frustrated quantum antiferromagnet Cs_2CuCl_4 , we start from the following spin-phonon Hamiltonian,

$$H = H_{\text{spin}}^{\text{pho}} + H^{\text{pho}}, \quad (2.1)$$

where the first term is of the form^{6,8,9}

$$H_{\text{spin}}^{\text{pho}} = \frac{1}{2} \sum_{ij} [J_{ij} \mathbf{S}_i \cdot \mathbf{S}_j + \mathbf{D}_{ij} \cdot (\mathbf{S}_i \times \mathbf{S}_j)] - \sum_i \mathbf{h} \cdot \mathbf{S}_i. \quad (2.2)$$

Here the \mathbf{S}_i are spin $S = 1/2$ operators at positions \mathbf{r}_i , the J_{ij} are the exchange energies connecting spins at positions \mathbf{r}_i and \mathbf{r}_j , the antisymmetric vectors \mathbf{D}_{ij} model the DM interaction, and \mathbf{h} is an external magnetic field. The second term in Eq. (2.1) describes noninteracting acoustic phonons,

$$H^{\text{pho}} = \sum_{\mathbf{k}\lambda} \omega_{\mathbf{k}\lambda} \left(a_{\mathbf{k}\lambda}^\dagger a_{\mathbf{k}\lambda} + \frac{1}{2} \right), \quad (2.3)$$

where $a_{\mathbf{k}\lambda}$ annihilates a phonon with wavevector \mathbf{k} and polarization λ , and the long-wavelength dispersion of the phonons is

$$\omega_{\mathbf{k}\lambda} = c_\lambda(\hat{\mathbf{k}})|\mathbf{k}|. \quad (2.4)$$

The velocities $c_\lambda(\hat{\mathbf{k}})$ of the phonons depend on their propagation direction $\hat{\mathbf{k}} = \mathbf{k}/|\mathbf{k}|$. The spin-phonon interaction in Eq. (2.2) arises from the fact that \mathbf{r}_i and \mathbf{r}_j are the actual positions of the spins for a given configuration of lattice distortions $\{\mathbf{X}_i\}$. Denoting by $\{\mathbf{R}_i\}$ the positions of the corresponding Bravais lattice, we have $\mathbf{r}_i = \mathbf{R}_i + \mathbf{X}_i$. The lattice distortions are quantized in the usual way,

$$\mathbf{X}_i = \frac{1}{\sqrt{N}} \sum_{\mathbf{k}} e^{i\mathbf{k}\cdot\mathbf{R}_i} \mathbf{X}_{\mathbf{k}}, \quad (2.5a)$$

$$\mathbf{X}_{\mathbf{k}} = \sum_{\lambda} X_{\mathbf{k}\lambda} \mathbf{e}_{\mathbf{k}\lambda}, \quad (2.5b)$$

$$X_{\mathbf{k}\lambda} = \frac{1}{\sqrt{2M\omega_{\mathbf{k}\lambda}}} (a_{\mathbf{k}\lambda} + a_{-\mathbf{k}\lambda}^\dagger), \quad (2.5c)$$

where the unit vectors $\mathbf{e}_{\mathbf{k}\lambda}$ define the polarization directions of the phonons. Introducing the momentum operators conjugate to the $X_{\mathbf{k}\lambda}$,

$$P_{\mathbf{k}\lambda} = \frac{1}{i} \sqrt{\frac{M\omega_{\mathbf{k}\lambda}}{2}} (a_{\mathbf{k}\lambda} - a_{-\mathbf{k}\lambda}^\dagger), \quad (2.6)$$

the pure phonon Hamiltonian (2.3) can be written as

$$H^{\text{pho}} = \sum_{\mathbf{k}\lambda} \left[\frac{P_{-\mathbf{k}\lambda} P_{\mathbf{k}\lambda}}{2M} + \frac{M}{2} \omega_{\mathbf{k}\lambda}^2 X_{-\mathbf{k}\lambda} X_{\mathbf{k}\lambda} \right]. \quad (2.7)$$

Assuming that positions of the spins deviate only slightly from their equilibrium values, we may expand the exchange couplings J_{ij} and the DM vectors \mathbf{D}_{ij} in powers of the difference vectors $\mathbf{X}_{ij} = \mathbf{X}_i - \mathbf{X}_j$,

$$J_{ij} = J(\mathbf{R}_{ij}) + (\mathbf{X}_{ij} \cdot \nabla_{\mathbf{r}}) J(\mathbf{r})|_{\mathbf{r}=\mathbf{R}_{ij}} + \frac{1}{2} (\mathbf{X}_{ij} \cdot \nabla_{\mathbf{r}})^2 J(\mathbf{r})|_{\mathbf{r}=\mathbf{R}_{ij}} + \dots, \quad (2.8a)$$

$$\mathbf{D}_{ij} = \mathbf{D}(\mathbf{R}_{ij}) + (\mathbf{X}_{ij} \cdot \nabla_{\mathbf{r}}) \mathbf{D}(\mathbf{r})|_{\mathbf{r}=\mathbf{R}_{ij}} + \frac{1}{2} (\mathbf{X}_{ij} \cdot \nabla_{\mathbf{r}})^2 \mathbf{D}(\mathbf{r})|_{\mathbf{r}=\mathbf{R}_{ij}} + \dots, \quad (2.8b)$$

where $\mathbf{R}_{ij} = \mathbf{R}_i - \mathbf{R}_j$ is again a vector of the Bravais lattice. Substituting the expansions (2.8a, 2.8b) into

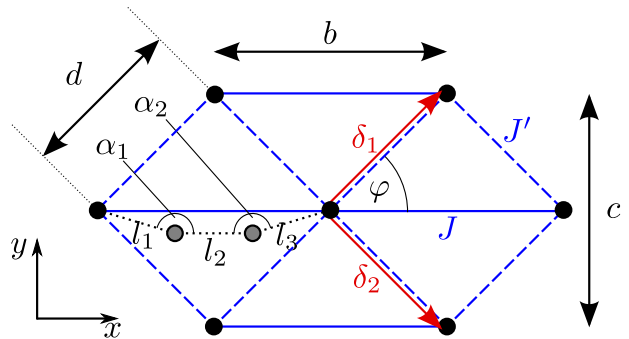


FIG. 1. (Color online) Triangular lattice with the lattice parameters b and c describing the geometry of a single layer of Cs_2CuCl_4 . The magnetic ions are located at the edges of the triangles (black dots) and are mainly coupled via the coupling J (solid line) in x -direction and J' along the diagonals (dashed line). The gray dots indicate the position of the chlorine atoms mediating the exchange interaction, which depends in a simple model on the three distances l_1, l_2, l_3 and on the two bonding angles α_1 and α_2 . For simplicity, we lump these dependencies into the variation of the bond length. In the same manner, also the dependence of the coupling J' on the angle φ is neglected.

Eq. (2.2) we obtain an expansion of our spin-phonon Hamiltonian in powers of the phonon operators,

$$H_{\text{spin}}^{\text{pho}} = H_{\text{spin}} + H_{\text{spin}}^{1\text{pho}} + H_{\text{spin}}^{2\text{pho}} + \dots, \quad (2.9)$$

where the pure spin part H_{spin} is obtained by assuming that the spins are located at the sites \mathbf{R}_i of the Bravais lattice, while the spin-phonon interactions $H_{\text{spin}}^{1\text{pho}}$ and $H_{\text{spin}}^{2\text{pho}}$ describe the coupling of one and two powers of the phonon operators \mathbf{X}_{ij} to the spin system.

The pure spin part H_{spin} of our spin-phonon Hamiltonian (2.9) which is formally identical with Eq. (2.2) except that now the spins are located at the sites \mathbf{R}_i of the Bravais lattice. From the values compiled in Tab. I it is clear that for the layered material Cs_2CuCl_4 the couplings between neighboring layers is very small^{6,27} so that we may ignore the interlayer coupling J'' and focus on a single layer. The spins are then located at the sites of a distorted triangular lattice characterized by the lattice parameters b and c , as shown in Fig. 1. Within the planes of the lattice, we assume an anisotropic nearest-neighbor exchange,^{6,8,9}

$$J_{ij} = J(\mathbf{R}_i - \mathbf{R}_j) = \begin{cases} J & \text{if } \mathbf{R}_i - \mathbf{R}_j = \pm(\boldsymbol{\delta}_1 + \boldsymbol{\delta}_2) \\ J' & \text{if } \mathbf{R}_i - \mathbf{R}_j = \pm\boldsymbol{\delta}_1 \text{ or } \pm\boldsymbol{\delta}_2 \end{cases}, \quad (2.10)$$

where

$$\boldsymbol{\delta}_1 = \frac{b}{2} \mathbf{e}_x + \frac{c}{2} \mathbf{e}_y, \quad (2.11a)$$

$$\boldsymbol{\delta}_2 = \frac{b}{2} \mathbf{e}_x - \frac{c}{2} \mathbf{e}_y, \quad (2.11b)$$

so that $\boldsymbol{\delta}_1 + \boldsymbol{\delta}_2 = b\mathbf{e}_x$ (see Fig. 1). The DM vectors \mathbf{D}_{ij} are assumed to point in the z -direction and connect sites

Parameter	Value (meV)
J	0.374(5)
J'	0.128(5)
J''	0.017(2)
D	0.020(2)

TABLE I. Accepted values^{6,8} of the in-plane exchange interactions J and J' , the inter-plane interaction J'' , and the Dzyaloshinskii–Moriya interaction D in Cs_2CuCl_4 . All comparisons between theory and experiment presented in this paper are based on these values. Note that the largest exchange coupling $J = 0.374$ meV corresponds to a temperature of 4.34 Kelvin.

in the directions $\pm\delta_1$ and $\pm\delta_2$,

$$\mathbf{D}_{ij} = D_{ij}\mathbf{e}_z = D(\mathbf{R}_i - \mathbf{R}_j)\mathbf{e}_z, \quad (2.12)$$

with $D_{ij} = -D_{ji}$ given by

$$D_{ij} = D(\mathbf{R}_i - \mathbf{R}_j) = \pm D \text{ if } \mathbf{R}_i - \mathbf{R}_j = \pm\delta_1 \text{ or } \pm\delta_2. \quad (2.13)$$

For Cs_2CuCl_4 , experimental estimates for J , J' , D , and the interlayer exchange coupling J'' are summarized in Tab. I. Throughout this paper, we assume that the external magnetic field is perpendicular to the plane of the lattice, $\mathbf{h} = h\mathbf{e}_z$. In the experimentally relevant regime $J' < 2J$ the spin system has then a unique classical ground state, as discussed in the following section. If the magnetic field lies in the plane of the lattice the ground state is more complicated and cannot be described within the framework of the spin-wave expansion used in this paper.¹⁷

B. Spin-wave expansion

1. General procedure

To set up the spin-wave expansion, we should first identify the ground-state spin configuration in the classical limit, where the spin operators are replaced by three-component classical vectors of length S , i.e., $\mathbf{S}_i \rightarrow S\hat{\mathbf{m}}_i$, where $\hat{\mathbf{m}}_i$ are unit vectors which point in the direction of the local magnetization.⁹ In the experimentally relevant regime $J' < 2J$ the classical ground state of our model is a spiral in the plane of the lattice, which is tilted towards the direction of the magnetic field. In this so-called “cone state” the magnetization points locally in the direction⁹

$$\hat{\mathbf{m}}_i = c_\theta[\cos(\mathbf{Q} \cdot \mathbf{R}_i)\mathbf{e}_x + \sin(\mathbf{Q} \cdot \mathbf{R}_i)\mathbf{e}_y] + s_\theta \mathbf{e}_z, \quad (2.14)$$

where we have introduced the abbreviation

$$s_\theta = \sin \theta, \quad c_\theta = \cos \theta. \quad (2.15)$$

This state is characterized by the opening angle θ of the cone and the wavevector \mathbf{Q} of the spiral, as shown

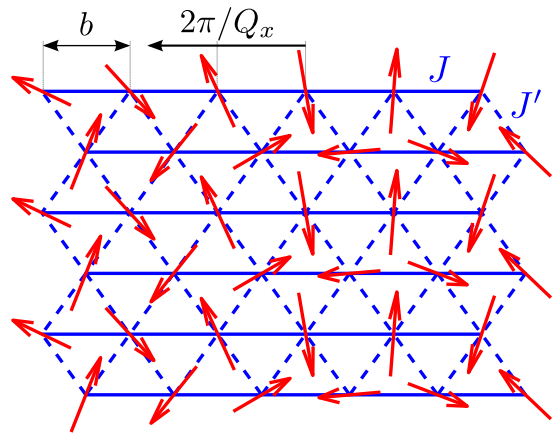


FIG. 2. (Color online) Projection of the graph of the “cone state”, which is the classical ground state of the anisotropic triangular lattice antiferromagnet for $J' < 2J$ and magnetic field perpendicular to the lattice plane. Note that the wavelength $2\pi/Q_x$ of the spiral has the indicated length and points along the x -axis in the direction of the arrow.

in Fig. 2. To bosonize our spin Hamiltonian using the Holstein–Primakoff transformation, we follow the general procedure outlined in Refs. [28 and 29] and complement the unit vectors $\hat{\mathbf{m}}_i$ by two orthogonal unit vectors $\mathbf{e}_i^{(1)}$ and $\mathbf{e}_i^{(2)}$ such that $\{\mathbf{e}_i^{(1)}, \mathbf{e}_i^{(2)}, \hat{\mathbf{m}}_i\}$ form a right-handed triad of orthogonal unit vectors for each site \mathbf{R}_i . The transverse basis vectors $\mathbf{e}_i^{(1)}$ and $\mathbf{e}_i^{(2)}$ are defined only up to a local $U(1)$ gauge transformation.²⁸ A convenient choice is

$$\mathbf{e}_i^{(1)} = \sin(\mathbf{Q} \cdot \mathbf{R}_i)\mathbf{e}_x - \cos(\mathbf{Q} \cdot \mathbf{R}_i)\mathbf{e}_y, \quad (2.16)$$

$$\mathbf{e}_i^{(2)} = s_\theta[\cos(\mathbf{Q} \cdot \mathbf{R}_i)\mathbf{e}_x + \sin(\mathbf{Q} \cdot \mathbf{R}_i)\mathbf{e}_y] - c_\theta \mathbf{e}_z. \quad (2.17)$$

Next we introduce the corresponding spherical basis vectors

$$\mathbf{e}_i^p = \mathbf{e}_i^{(1)} + ip\mathbf{e}_i^{(2)}, \quad p = \pm, \quad (2.18)$$

and expand the spin operators in this basis,

$$\mathbf{S}_i = S_i^\parallel \hat{\mathbf{m}}_i + \mathbf{S}_i^\perp, \quad (2.19)$$

with the transverse part given by

$$\mathbf{S}_i^\perp = \frac{1}{2} \sum_{p=\pm} S_i^{-p} \mathbf{e}_i^p. \quad (2.20)$$

The spin components are then bosonized using the Holstein–Primakoff transformation,

$$S_i^\parallel = S - n_i, \quad (2.21a)$$

$$S_i^+ = \sqrt{2S} \sqrt{1 - \frac{n_i}{2S}} b_i, \quad (2.21b)$$

$$S_i^- = \sqrt{2S} b_i^\dagger \sqrt{1 - \frac{n_i}{2S}}, \quad (2.21c)$$

where $n_i = b_i^\dagger b_i$ and b_i are canonical boson operators. The bosonized spin part of our Hamiltonian can then be written as

$$H_{\text{spin}} = H_0 + H_{2\parallel} + H_{4\parallel} + H_{\perp} + H_{\parallel\perp}, \quad (2.22)$$

where

$$H_0 = \frac{S^2}{2} \sum_{ij} J_{ij}^{\parallel} - S \sum_i \mathbf{h} \cdot \hat{\mathbf{m}}_i, \quad (2.23)$$

$$H_{2\parallel} = -\frac{S}{2} \sum_{ij} J_{ij}^{\parallel} (n_i + n_j) + \sum_i \mathbf{h} \cdot \hat{\mathbf{m}}_i n_i, \quad (2.24)$$

$$H_{4\parallel} = \frac{1}{2} \sum_{ij} J_{ij}^{\parallel} n_i n_j, \quad (2.25)$$

$$\begin{aligned} H_{\perp} &= \frac{1}{2} \sum_{ij} [J_{ij} \mathbf{S}_i^{\perp} \cdot \mathbf{S}_j^{\perp} + \mathbf{D}_{ij} \cdot (\mathbf{S}_i^{\perp} \times \mathbf{S}_j^{\perp})] \\ &= \frac{1}{8} \sum_{ij} \sum_{pp'} J_{ij}^{pp'} S_i^{-p} S_j^{-p'}, \end{aligned} \quad (2.26)$$

$$\begin{aligned} H_{\parallel\perp} &= \sum_{ij} \mathbf{S}_i^{\perp} \cdot [(J_{ij} - \mathbf{D}_{ij} \times) \hat{\mathbf{m}}_j (S - n_j) - \delta_{ij} \mathbf{h}] \\ &= -\sum_{ij} \mathbf{S}_i^{\perp} \cdot [(J_{ij} - \mathbf{D}_{ij} \times) \hat{\mathbf{m}}_j n_j], \end{aligned} \quad (2.27)$$

where in the last line we have used the fact that the spin configuration in the classical ground state satisfies²⁸

$$\hat{\mathbf{m}}_i \times \left[\mathbf{h} - S \sum_j (J_{ij} - \mathbf{D}_{ij} \times) \hat{\mathbf{m}}_j \right] = 0. \quad (2.28)$$

For simplicity we have introduced the following effective couplings between longitudinal and transverse spin fluctuations,

$$J_{ij}^{\parallel} = J_{ij} \hat{\mathbf{m}}_i \cdot \hat{\mathbf{m}}_j + \mathbf{D}_{ij} \cdot (\hat{\mathbf{m}}_i \times \hat{\mathbf{m}}_j), \quad (2.29a)$$

$$J_{ij}^{pp'} = J_{ij} (\mathbf{e}_i^p \cdot \mathbf{e}_j^{p'}) + \mathbf{D}_{ij} \cdot (\mathbf{e}_i^p \times \mathbf{e}_j^{p'}). \quad (2.29b)$$

Defining $\varphi_i = \mathbf{Q} \cdot \mathbf{R}_i$ and $\varphi_{ij} = \varphi_i - \varphi_j = \mathbf{Q} \cdot (\mathbf{R}_i - \mathbf{R}_j)$, we obtain with our choice of basis

$$J_{ij}^{\parallel} = J_{ij} [s_{\theta}^2 + c_{\theta}^2 \cos \varphi_{ij}] - D_{ij} c_{\theta}^2 \sin \varphi_{ij}, \quad (2.30a)$$

$$\begin{aligned} J_{ij}^{+-} &= (J_{ij}^{-+})^* \\ &= J_{ij} [c_{\theta}^2 + (1 + s_{\theta}^2) \cos \varphi_{ij} - 2is_{\theta} \sin \varphi_{ij}] \\ &\quad - D_{ij} [(1 + s_{\theta}^2) \sin \varphi_{ij} + 2is_{\theta} \cos \varphi_{ij}], \end{aligned} \quad (2.30b)$$

$$\begin{aligned} J_{ij}^{++} &= J_{ij}^{--} \\ &= -c_{\theta}^2 [J_{ij} (1 - \cos \varphi_{ij}) + D_{ij} \sin \varphi_{ij}]. \end{aligned} \quad (2.30c)$$

It is convenient to introduce the Fourier transforms of the exchange couplings and the DM interaction:

$$\begin{aligned} J_{\mathbf{k}} &= \sum_{\mathbf{R}} e^{-i\mathbf{k} \cdot \mathbf{R}} J(\mathbf{R}) \\ &= 2J \cos(k_x b) + 4J' \cos(k_x b/2) \cos(k_y c/2), \end{aligned} \quad (2.31)$$

$$\begin{aligned} D_{\mathbf{k}} &= \sum_{\mathbf{R}} e^{-i\mathbf{k} \cdot \mathbf{R}} D(\mathbf{R}) \\ &= -4iD \sin(k_x b/2) \cos(k_y c/2). \end{aligned} \quad (2.32)$$

We also define the combination

$$J_{\mathbf{k}}^D = J_{\mathbf{k}} - iD_{\mathbf{k}}, \quad (2.33)$$

which is real because the Fourier transform of the DM coupling $D_{\mathbf{k}}$ is purely imaginary. The Fourier transforms of the effective couplings (2.30a-2.30c) can then be written as

$$J_{\mathbf{k}}^{\parallel} = s_{\theta}^2 J_{\mathbf{k}} + c_{\theta}^2 \frac{J_{\mathbf{Q}+\mathbf{k}}^D + J_{\mathbf{Q}-\mathbf{k}}^D}{2}, \quad (2.34a)$$

$$\begin{aligned} J_{\mathbf{k}}^{+-} = J_{-\mathbf{k}}^{-+} &= c_{\theta}^2 J_{\mathbf{k}} + (1 + s_{\theta}^2) \frac{J_{\mathbf{Q}+\mathbf{k}}^D + J_{\mathbf{Q}-\mathbf{k}}^D}{2} \\ &\quad + s_{\theta} [J_{\mathbf{Q}+\mathbf{k}}^D - J_{\mathbf{Q}-\mathbf{k}}^D], \end{aligned} \quad (2.34b)$$

$$J_{\mathbf{k}}^{++} = J_{\mathbf{k}}^{--} = -c_{\theta}^2 \left[J_{\mathbf{k}} - \frac{J_{\mathbf{Q}+\mathbf{k}}^D + J_{\mathbf{Q}-\mathbf{k}}^D}{2} \right]. \quad (2.34c)$$

2. Classical ground state: Cone state

To fix the parameters θ and \mathbf{Q} which characterize the classical ground state, we substitute Eq. (2.30a) into our expression (2.23) for the classical ground-state energy and minimize with respect to θ and \mathbf{Q} . The classical ground-state energy can then be written as

$$\begin{aligned} H_0 &= N \frac{S^2}{2} J_{\mathbf{k}=0}^{\parallel} - N S h s_{\theta} \\ &= N \frac{S^2}{2} [s_{\theta}^2 J_{\mathbf{k}=0} + c_{\theta}^2 J_{\mathbf{Q}}^D] - N S h s_{\theta}. \end{aligned} \quad (2.35)$$

Minimizing this with respect to θ we obtain

$$s_{\theta} \equiv \sin \theta = h/h_c, \quad (2.36)$$

where the critical magnetic field is given by

$$h_c = S(J_0^D - J_{\mathbf{Q}}^D) = S(J_0 - J_{\mathbf{Q}} + iD_{\mathbf{Q}}). \quad (2.37)$$

The wavevector of the spiral is obtained by minimizing H_0 in Eq. (2.35) with respect to \mathbf{Q} , which amounts to finding the minimum of the real function $J_{\mathbf{Q}}^D$. The wavevector of the spiral is thus determined:

$$\nabla_{\mathbf{Q}} J_{\mathbf{Q}}^D \equiv \nabla_{\mathbf{k}} (J_{\mathbf{k}} - iD_{\mathbf{k}})_{\mathbf{k}=\mathbf{Q}} = 0. \quad (2.38)$$

Anticipating that this condition leads to a spiral along the x -axis, $\mathbf{Q} = Q_x \mathbf{e}_x$, and using the above expressions for $J_{\mathbf{k}}$ and $D_{\mathbf{k}}$, it is easy to show that Eq. (2.38) reduces to the following transcendental equation for $x = Q_x b$:

$$\cos\left(\frac{x}{2}\right) = -\frac{J'}{2J} - \frac{D}{2J} \cot\left(\frac{x}{2}\right). \quad (2.39)$$

Note that for $D = 0$ and isotropic exchange couplings ($J' = J$) this condition reduces to $\cos(x/2) = -1/2$, implying $x = Q_x b = 4\pi/3$, which describes the usual 120° ground state of an isotropic triangular lattice antiferromagnet.

3. Magnon dispersion

To calculate the magnon spectrum to leading order in the $1/S$ expansion, we may approximate $S_i^+ \approx \sqrt{2S}b_i$ and $S_i^- \approx \sqrt{2S}b_i^\dagger$, so that the transverse part of our spin-wave Hamiltonian is approximated by $H_\perp \approx H_{2\perp}$ with

$$H_{2\perp} = \frac{S}{4} \sum_{ij} [J_{ij}^{+-} b_i^\dagger b_j + J_{ij}^{-+} b_i b_j^\dagger + J_{ij}^{++} b_i^\dagger b_j^\dagger + J_{ij}^{--} b_i b_j]. \quad (2.40)$$

The magnon spectrum can then be obtained by diagonalizing the quadratic boson Hamiltonian $H_2 = H_{2\parallel} + H_{2\perp}$. Combining Eqs. (2.24) and (2.40) we obtain

$$H_2 = \frac{S}{2} \sum_{ij} \left\{ -J_{ij}^\parallel (n_i + n_j) + \frac{1}{2} [J_{ij}^{+-} b_i^\dagger b_j + J_{ij}^{-+} b_i b_j^\dagger + J_{ij}^{++} b_i^\dagger b_j^\dagger + J_{ij}^{--} b_i b_j] \right\} + h s_\theta \sum_i n_i. \quad (2.41)$$

Introducing the Fourier transform of the boson operators via

$$b_i = \frac{1}{\sqrt{N}} \sum_{\mathbf{k}} e^{i\mathbf{k}\cdot\mathbf{R}_i} b_{\mathbf{k}}, \quad (2.42)$$

we obtain in momentum space,

$$H_2 = \sum_{\mathbf{k}} \left\{ A_{\mathbf{k}} b_{\mathbf{k}}^\dagger b_{\mathbf{k}} + \frac{B_{\mathbf{k}}}{2} [b_{\mathbf{k}}^\dagger b_{-\mathbf{k}}^\dagger + b_{-\mathbf{k}} b_{\mathbf{k}}] \right\}, \quad (2.43)$$

where $A_{\mathbf{k}} = A_{\mathbf{k}}^+ + A_{\mathbf{k}}^-$, with

$$A_{\mathbf{k}}^+ = -B_{\mathbf{k}} - S \left[J_Q^D - \frac{J_{Q+\mathbf{k}}^D + J_{Q-\mathbf{k}}^D}{2} \right], \quad (2.44a)$$

$$A_{\mathbf{k}}^- = S s_\theta \frac{J_{Q+\mathbf{k}}^D - J_{Q-\mathbf{k}}^D}{2}, \quad (2.44b)$$

$$B_{\mathbf{k}} = -\frac{S}{2} c_\theta^2 \left[J_{\mathbf{k}} - \frac{J_{Q+\mathbf{k}}^D + J_{Q-\mathbf{k}}^D}{2} \right]. \quad (2.44c)$$

These coefficients are real and have the symmetries $A_{-\mathbf{k}}^\pm = \pm A_{\mathbf{k}}^\pm$ and $B_{\mathbf{k}} = B_{-\mathbf{k}}$. Note that

$$B_0 = -\frac{S}{2} c_\theta^2 [J_0 - J_Q^D] = -\frac{c_\theta^2}{2} h_c, \quad (2.45a)$$

$$A_0 = \frac{c_\theta^2}{2} h_c, \quad (2.45b)$$

which implies that the magnon dispersion is gapless at $\mathbf{k} = 0$, as required by the $U(1)$ -symmetry of the Hamiltonian. Note also that for small \mathbf{k} the linear coefficient in the Taylor expansion of the antisymmetric coefficient $A_{\mathbf{k}}^-$ vanishes due to Eqs. (2.33) and (2.38), so that

$$A_{\mathbf{k}}^- = \mathcal{O}(\mathbf{k}^3). \quad (2.46)$$

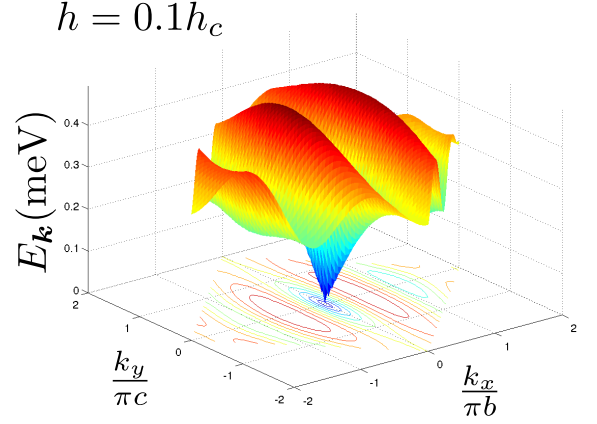


FIG. 3. (Color online) Graph of the magnon dispersion $E_{\mathbf{k}}$ of the anisotropic triangular lattice antiferromagnet Cs_2CuCl_4 with $J'/J = 0.34$, Dzyaloshinskii–Moriya anisotropy $D/J = 0.054$, and for a magnetic field $h = 0.1h_c$; see Eq. (2.50). Note that the $U(1)$ -symmetry of the Hamiltonian guarantees that for $\mathbf{k} = 0$ the magnon dispersion is gapless.⁹

To obtain the magnon dispersion, we diagonalize the Hamiltonian (2.43) using the following canonical (Bogoliubov) transformation,

$$\begin{pmatrix} b_{\mathbf{k}} \\ b_{-\mathbf{k}}^\dagger \end{pmatrix} = \begin{pmatrix} u_{\mathbf{k}} & -v_{\mathbf{k}} \\ -v_{\mathbf{k}} & u_{\mathbf{k}} \end{pmatrix} \begin{pmatrix} \beta_{\mathbf{k}} \\ \beta_{-\mathbf{k}}^\dagger \end{pmatrix}, \quad (2.47)$$

where

$$u_{\mathbf{k}} = \sqrt{\frac{A_{\mathbf{k}}^+ + \epsilon_{\mathbf{k}}}{2\epsilon_{\mathbf{k}}}}, \quad v_{\mathbf{k}} = \frac{B_{\mathbf{k}}}{|B_{\mathbf{k}}|} \sqrt{\frac{A_{\mathbf{k}}^+ - \epsilon_{\mathbf{k}}}{2\epsilon_{\mathbf{k}}}}, \quad (2.48)$$

and

$$\epsilon_{\mathbf{k}} = \sqrt{(A_{\mathbf{k}}^+)^2 - B_{\mathbf{k}}^2}. \quad (2.49)$$

The energy $\epsilon_{\mathbf{k}} = \epsilon_{-\mathbf{k}}$ is even under $\mathbf{k} \rightarrow -\mathbf{k}$; the full magnon dispersion is

$$E_{\mathbf{k}} = \epsilon_{\mathbf{k}} + A_{\mathbf{k}}^- = \sqrt{(A_{\mathbf{k}}^+)^2 - B_{\mathbf{k}}^2} + A_{\mathbf{k}}^-, \quad (2.50)$$

which does not have any definite symmetry with respect to $\mathbf{k} \rightarrow -\mathbf{k}$. The diagonalized form of the magnon Hamiltonian reads

$$H_2 = \sum_{\mathbf{k}} \left[E_{\mathbf{k}} \beta_{\mathbf{k}}^\dagger \beta_{\mathbf{k}} + \frac{\epsilon_{\mathbf{k}} - A_{\mathbf{k}}^+}{2} \right]. \quad (2.51)$$

A graph of the magnon dispersion $E_{\mathbf{k}}$ is shown in Fig. 3. Using the fact that according to Eq. (2.46) the term $A_{\mathbf{k}}^-$ can be neglected for small \mathbf{k} , the leading long-wavelength limit of the magnon dispersion is

$$E_{\mathbf{k}} = \sqrt{v_x^2 k_x^2 + v_y^2 k_y^2} + \mathcal{O}(\mathbf{k}^3) = v(\hat{\mathbf{k}}) |\mathbf{k}| + \mathcal{O}(\mathbf{k}^3), \quad (2.52)$$

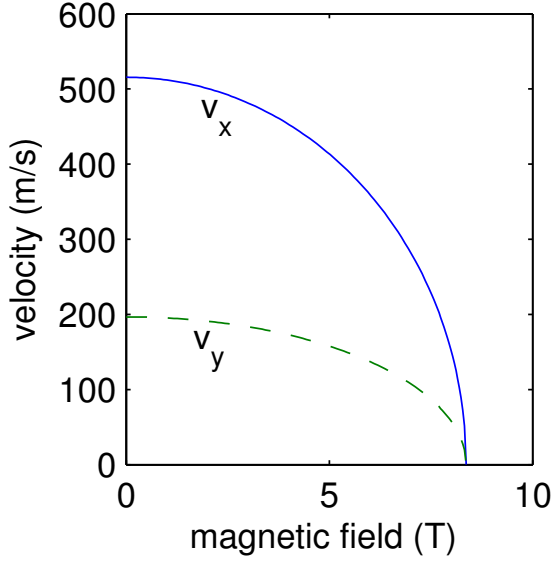


FIG. 4. (Color online) Plot of the linear spin-wave result for the magnon velocities of Cs_2CuCl_4 in the two principal directions of the lattice as a function of the magnetic field. The relevant values of J , J' , and D are given in Tab. I. It turns out that for an arbitrary magnetic field the magnon velocities are small compared with the velocities c_λ of acoustic phonons in Cs_2CuCl_4 .

with direction-dependent magnon velocity

$$v(\hat{\mathbf{k}}) = \sqrt{v_x^2 \hat{k}_x^2 + v_y^2 \hat{k}_y^2}, \quad (2.53)$$

where $\hat{\mathbf{k}} = \mathbf{k}/|\mathbf{k}|$. In Fig. 4 we show a graph of the linear spin-wave result of the two principal magnon velocities v_x and v_y as a function of the external magnetic field for Cs_2CuCl_4 , where J , J' , and D have the values given in Tab. I.

4. Interactions between magnons

The terms in the transverse Hamiltonian H_\perp involving more than two boson operators and the contributions $H_{4\parallel}$ and $H_{\perp\perp}$ to the magnon Hamiltonian given in Eqs. (2.25) and (2.27) describe various interaction processes between magnons. As compared with the S -dependence of the free magnon dispersion $E_{\mathbf{k}} \propto S$, the interaction contains higher orders of the small parameter $1/S$, so that at first sight it seems that for large S we can simply neglect interaction effects. It turns out, however, that for the proper calculation of the long-wavelength limit of the ultrasonic attenuation rate the leading contribution H_3 to the mixing term $H_{\perp\perp}$ involving three magnon operators cannot be neglected. This part of the magnon Hamiltonian can be written as

$$H_3 = -c_\theta \frac{\sqrt{2S}}{2i} \sum_{ij} \left[K_{ij} b_i^\dagger b_j^\dagger b_j - K_{ij}^* b_j^\dagger b_i b_i \right], \quad (2.54)$$

where we have defined

$$K_{ij} = s_\theta [J_{ij}(1 - \cos \varphi_{ij}) + D_{ij} \sin \varphi_{ij}] + i [J_{ij} \sin \varphi_{ij} + D_{ij} \cos \varphi_{ij}]. \quad (2.55)$$

In momentum space H_3 can be written as

$$H_3 = \frac{1}{\sqrt{N}} \sum_{\mathbf{k}_1 \mathbf{k}_2 \mathbf{k}_3} \delta_{\mathbf{k}_1 + \mathbf{k}_2 + \mathbf{k}_3, 0} \left[\frac{1}{2!} \Gamma_3^{b^\dagger b^\dagger b}(\mathbf{k}_1, \mathbf{k}_2; \mathbf{k}_3) b_{-\mathbf{k}_1}^\dagger b_{-\mathbf{k}_2}^\dagger b_{\mathbf{k}_3} + \frac{1}{2!} \Gamma_3^{b^\dagger bb}(\mathbf{k}_1; \mathbf{k}_2, \mathbf{k}_3) b_{-\mathbf{k}_1}^\dagger b_{\mathbf{k}_2} b_{\mathbf{k}_3} \right], \quad (2.56)$$

with the vertices given by

$$\Gamma_3^{b^\dagger b^\dagger b}(\mathbf{k}_1, \mathbf{k}_2; \mathbf{k}_3) = -c_\theta \frac{\sqrt{2S}}{2i} [K_{-\mathbf{k}_1} + K_{-\mathbf{k}_2}], \quad (2.57a)$$

$$\Gamma_3^{b^\dagger bb}(\mathbf{k}_1; \mathbf{k}_2, \mathbf{k}_3) = c_\theta \frac{\sqrt{2S}}{2i} [K_{\mathbf{k}_2} + K_{\mathbf{k}_3}], \quad (2.57b)$$

where $K_{\mathbf{k}}$ is the Fourier transform of the function K_{ij} defined in Eq. (2.55):

$$K_{\mathbf{k}} = s_\theta \left[J_{\mathbf{k}} - \frac{J_{\mathbf{Q}+\mathbf{k}}^D + J_{\mathbf{Q}-\mathbf{k}}^D}{2} \right] - \frac{J_{\mathbf{Q}+\mathbf{k}}^D - J_{\mathbf{Q}-\mathbf{k}}^D}{2}. \quad (2.58)$$

For later reference we note that

$$K_0 = s_\theta (J_0 - J_{\mathbf{Q}}^D) = s_\theta \frac{h_c}{S}. \quad (2.59)$$

C. Magnon-phonon interactions

1. Modeling the derivatives of the exchange couplings in Cs_2CuCl_4

Substituting the gradient expansions (2.8a) and (2.8b) for the exchange and DM couplings into the spin-phonon Hamiltonian $H_{\text{spin}}^{\text{pho}}$ defined in Eq. (2.2), we obtain an expansion of $H_{\text{spin}}^{\text{pho}}$ in powers of the phonon operators of the form (2.9). Since the exchange interactions are large compared with the DM interactions, we shall neglect the dependence of the DM couplings \mathbf{D}_{ij} in the phonon coordinates. The n -phonon part of our spin-phonon Hamiltonian can be written as

$$H_{\text{spin}}^{n\text{pho}} = \frac{1}{2} \sum_{ij} U_{ij}^{(n)} \mathbf{S}_i \cdot \mathbf{S}_j, \quad (2.60)$$

where the coupling functions involving $n = 1$ and $n = 2$ phonons are

$$U_{ij}^{(1)} = (\mathbf{X}_{ij} \cdot \nabla_{\mathbf{r}}) J(\mathbf{r})|_{\mathbf{r}=\mathbf{R}_{ij}} \equiv \mathbf{X}_{ij} \cdot \mathbf{J}_{ij}^{(1)}, \quad (2.61)$$

$$U_{ij}^{(2)} = \frac{1}{2} (\mathbf{X}_{ij} \cdot \nabla_{\mathbf{r}})^2 J(\mathbf{r})|_{\mathbf{r}=\mathbf{R}_{ij}} \equiv \frac{1}{2} \mathbf{X}_{ij}^T \mathbf{J}_{ij}^{(2)} \mathbf{X}_{ij}, \quad (2.62)$$

with the vector $\mathbf{J}_{ij}^{(1)}$ and the tensor $\mathbf{J}_{ij}^{(2)}$ defined by

$$\mathbf{J}_{ij}^{(1)} \equiv \mathbf{J}^{(1)}(\mathbf{R}_{ij}) = \nabla_{\mathbf{r}} J(\mathbf{r})|_{\mathbf{r}=\mathbf{R}_{ij}}, \quad (2.63)$$

$$[\mathbf{J}_{ij}^{(2)}]_{\alpha\beta} \equiv [\mathbf{J}^{(2)}(\mathbf{R}_{ij})]_{\alpha\beta} = \left. \frac{J(\mathbf{r})}{\partial r_{\alpha} \partial r_{\beta}} \right|_{\mathbf{r}=\mathbf{R}_{ij}}. \quad (2.64)$$

The Fourier transforms of functions (2.61) and (2.62) are

$$\begin{aligned} U_{\mathbf{k},\mathbf{k}'}^{(1)} &= \frac{1}{N} \sum_{ij} e^{-i\mathbf{k}\cdot\mathbf{R}_i - i\mathbf{k}'\cdot\mathbf{R}_j} U_{ij}^{(1)} \\ &= -\frac{1}{\sqrt{N}} \mathbf{X}_{\mathbf{k}+\mathbf{k}'} \cdot (\mathbf{J}_{\mathbf{k}}^{(1)} + \mathbf{J}_{\mathbf{k}'}^{(1)}), \end{aligned} \quad (2.65)$$

$$\begin{aligned} U_{\mathbf{k},\mathbf{k}'}^{(2)} &= \frac{1}{N} \sum_{ij} e^{-i\mathbf{k}\cdot\mathbf{R}_i - i\mathbf{k}'\cdot\mathbf{R}_j} U_{ij}^{(2)} \\ &= \frac{1}{2N} \sum_{\mathbf{q}} \mathbf{X}_{\mathbf{q}}^{\dagger} (\mathbf{J}_{\mathbf{k}}^{(2)} - \mathbf{J}_{\mathbf{k}+\mathbf{q}}^{(2)} + \mathbf{J}_{\mathbf{k}'}^{(2)} - \mathbf{J}_{\mathbf{k}'+\mathbf{q}}^{(2)}) \mathbf{X}_{\mathbf{q}+\mathbf{k}+\mathbf{k}'}, \end{aligned} \quad (2.66)$$

where

$$\mathbf{J}_{\mathbf{k}}^{(1)} = \sum_{\mathbf{R}} e^{-i\mathbf{k}\cdot\mathbf{R}} \mathbf{J}^{(1)}(\mathbf{R}), \quad (2.67)$$

and similarly for $\mathbf{J}_{\mathbf{k}}^{(2)}$. Note that the Fourier transform $\mathbf{J}_{\mathbf{k}}^{(1)}$ of the gradient has the symmetries

$$\mathbf{J}_{-\mathbf{k}}^{(1)} = -\mathbf{J}_{\mathbf{k}}^{(1)} = (\mathbf{J}_{\mathbf{k}}^{(1)})^*, \quad (2.68)$$

which implies that $\mathbf{J}_{\mathbf{k}}^{(1)}$ is purely imaginary and vanishes for $\mathbf{k} = 0$. In contrast, the second derivative tensor is an even function of \mathbf{k} ,

$$\mathbf{J}_{-\mathbf{k}}^{(2)} = \mathbf{J}_{\mathbf{k}}^{(2)}, \quad (2.69)$$

and thus has a finite limit at zero momentum. In general, in-plane lattice deformations in Cs_2CuCl_4 induce changes in both couplings J and J' as indicated in Fig. 1. In principle one should use four independent parameters to describe the changes of J and J' in response to the displacement of the lattice sites in two independent in-plane directions. To reduce the parameter space, we note that usually the exchange couplings originate from an electronic exchange path where orbitals of neighboring atoms overlap. For Cs_2CuCl_4 the exchange is mediated by the chlorine atoms located in between the copper atoms, as shown in Fig. 1. In a rough approximation where only the coupling of a few atoms is considered, the exchange couplings do not change to first order in the displacements when one of the copper atoms moves up or down. Therefore one can neglect the variation of J with respect to displacements in the y -direction and assume that J only changes appreciably if the atoms move in the x -direction. By a similar argument one can also neglect the dependence of the coupling $J'(\mathbf{r}) = J'(r, \varphi)$ on the polar angle φ , setting

$$\frac{\partial J'}{\partial x} = \cos \varphi_0 \frac{\partial J'}{\partial r}, \quad \frac{\partial J'}{\partial y} = \sin \varphi_0 \frac{\partial J'}{\partial r}, \quad (2.70)$$

where $\sin \varphi_0 = c/(2d)$. Here $d = \sqrt{b^2 + c^2}/2$ is the relevant bond length, and $\partial J'/\partial r$ is the derivative of the coupling J' with respect to the distance between the spins. With these approximations we obtain the following expression for the gradient $\mathbf{J}_{\mathbf{k}}^{(1)}$ of the exchange couplings in Cs_2CuCl_4 :

$$\begin{aligned} \mathbf{J}_{\mathbf{k}}^{(1)} &= -2i \frac{\partial J}{\partial x} e_x \sin(k_x b) \\ &\quad - 4i \frac{\partial J'}{\partial r} \left[e_x \cos \varphi_0 \sin(k_x b/2) \cos(k_y c/2) \right. \\ &\quad \left. + e_y \sin \varphi_0 \cos(k_x b/2) \sin(k_y c/2) \right]. \end{aligned} \quad (2.71)$$

Similarly, we obtain for the matrix elements of the second derivative tensor $\mathbf{J}_{\mathbf{k}}^{(2)} = \mathbf{J}_{\mathbf{k}}^{(2)T}$,

$$\begin{aligned} [\mathbf{J}_{\mathbf{k}}^{(2)}]_{11} &= 2 \cos(k_x b) \frac{\partial^2 J}{\partial x^2} \\ &\quad + 4 \cos^2 \varphi_0 \cos(k_x b/2) \cos(k_y c/2) \frac{\partial^2 J'}{\partial r^2}, \end{aligned} \quad (2.72a)$$

$$[\mathbf{J}_{\mathbf{k}}^{(2)}]_{12} = 4 \cos \varphi_0 \sin \varphi_0 \sin(k_x b/2) \sin(k_y c/2) \frac{\partial^2 J'}{\partial r^2}, \quad (2.72b)$$

$$[\mathbf{J}_{\mathbf{k}}^{(2)}]_{22} = 4 \sin^2 \varphi_0 \cos(k_x b/2) \cos(k_y c/2) \frac{\partial^2 J'}{\partial r^2}. \quad (2.72c)$$

Due to the $U(1)$ -symmetry of the Hamiltonian, the vector $\mathbf{J}_{\mathbf{k}}^{(1)}$ and the tensor $\mathbf{J}_{\mathbf{k}}^{(2)}$ are only fixed up to a phase that depends on the choice of triad $\{\mathbf{e}_i^{(1)}, \mathbf{e}_i^{(2)}, \hat{\mathbf{m}}_i\}$; see Ref. [28] for a discussion of this point. Note that the geometry shown in Fig. 1 suggests that the couplings will become stronger if the bond length is enlarged; at first sight this counterintuitive behavior originates from the fact that the bond angles between the chlorine atoms become larger with increasing bond length, which usually results in a stronger coupling.³⁰ Later we will see that only the squares of the derivatives enter in the final result for the velocity shifts and the ultrasonic attenuation rates, so that one cannot directly determine the sign of the change of the coupling strengths from the ultrasound measurements.

2. Phonon renormalization in the classical spin background

Expanding the spin operators in Eq. (2.60) in powers of Holstein–Primakoff bosons, we obtain a double expansion of the spin-phonon Hamiltonian in powers of phonon operators and magnon operators. For our purpose, it is sufficient to retain only terms up to two phonon operators. After expressing the spin operators in Eq. (2.60) in terms of Holstein–Primakoff bosons, to leading order for large S , we generate also pure phonon contributions of the form

$$H_0^{\text{npho}} = \frac{S^2}{2} \sum_{ij} U_{ij}^{(n)} \hat{\mathbf{m}}_i \cdot \hat{\mathbf{m}}_j, \quad (2.73)$$

which describe motion of n phonons in the classical spin background. In particular, the one-phonon term $H_0^{1\text{pho}}$ can be written as

$$H_0^{1\text{pho}} = \frac{S^2}{2} \left[s_\theta^2 U_{0,0}^{(1)} + \frac{c_\theta^2}{2} \left(U_{-\mathbf{Q},\mathbf{Q}}^{(1)} + U_{\mathbf{Q},-\mathbf{Q}}^{(1)} \right) \right]. \quad (2.74)$$

But from Eqs. (2.65) and (2.68) we see that $U_{0,0}^{(1)} = U_{-\mathbf{Q},\mathbf{Q}}^{(1)} = 0$, implying $H_0^{1\text{pho}} = 0$. On the other hand, the corresponding two-phonon part

$$H_0^{2\text{pho}} = \frac{S^2}{2} \left[s_\theta^2 U_{0,0}^{(2)} + \frac{c_\theta^2}{2} \left(U_{-\mathbf{Q},\mathbf{Q}}^{(2)} + U_{\mathbf{Q},-\mathbf{Q}}^{(2)} \right) \right] \quad (2.75)$$

is finite and yields an important contribution to the magnetic field dependence of the elastic constants. Inserting the explicit expression for the Fourier transform $U_{\mathbf{k},\mathbf{k}'}^{(2)}$ of the second derivative couplings $U_{ij}^{(2)}$ [see Eqs. (2.62) and (2.66)] and using the symmetry Eq. (2.69) we see that Eq. (2.75) can be written as

$$H_0^{2\text{pho}} = \frac{M}{2} \sum_{\mathbf{k}\lambda} \Sigma_0^{\text{pho}}(\mathbf{k}, \lambda) X_{-\mathbf{k}\lambda} X_{\mathbf{k}\lambda}, \quad (2.76)$$

where the zeroth order contribution to the phonon self-energy (in an expansion in powers of the magnon operators) is given by

$$\Sigma_0^{\text{pho}}(\mathbf{k}, \lambda) = \frac{S^2}{M} \mathbf{e}_{\mathbf{k}\lambda}^\dagger \left[s_\theta^2 \left(\mathbf{J}_0^{(2)} - \mathbf{J}_{\mathbf{k}}^{(2)} \right) + c_\theta^2 \mathbf{J}_{\mathbf{Q},\mathbf{k}}^{(2+)} \right] \mathbf{e}_{\mathbf{k}\lambda}. \quad (2.77)$$

Here we have defined

$$\mathbf{J}_{\mathbf{k},\mathbf{Q}}^{(2+)} = \mathbf{J}_{\mathbf{k}}^{(2)} - \frac{\mathbf{J}_{\mathbf{k}+\mathbf{Q}}^{(2)} + \mathbf{J}_{\mathbf{k}-\mathbf{Q}}^{(2)}}{2}. \quad (2.78a)$$

For later convenience we also introduce the notation

$$\mathbf{J}_{\mathbf{k},\mathbf{Q}}^{(2-)} = \frac{\mathbf{J}_{\mathbf{k}+\mathbf{Q}}^{(2)} - \mathbf{J}_{\mathbf{k}-\mathbf{Q}}^{(2)}}{2}. \quad (2.78b)$$

Keeping in mind that $\mathbf{J}_{\mathbf{k}}^{(2)}$ is an even function of \mathbf{k} , we see that $\mathbf{J}_{\mathbf{k},\mathbf{Q}}^{(2+)}$ is even while $\mathbf{J}_{\mathbf{k},\mathbf{Q}}^{(2-)}$ is odd under $\mathbf{k} \rightarrow -\mathbf{k}$,

$$\mathbf{J}_{\mathbf{k},\mathbf{Q}}^{(2\pm)} = \pm \mathbf{J}_{-\mathbf{k},\mathbf{Q}}^{(2\pm)}. \quad (2.79)$$

3. One-phonon one-magnon hybridization

The part $H_{1\text{mag}}^{1\text{pho}}$ of our spin-phonon Hamiltonian involving one phonon and one magnon operator is given by

$$H_{1\text{mag}}^{1\text{pho}} = \frac{(2S)^{3/2}}{4} \sum_{ij} U_{ij}^{(1)} \left[b_i^\dagger (\mathbf{e}_i^+ \cdot \hat{\mathbf{m}}_j) + b_i (\mathbf{e}_i^- \cdot \hat{\mathbf{m}}_j) \right]. \quad (2.80)$$

Using

$$\mathbf{e}_i^\pm \cdot \hat{\mathbf{m}}_j = c_\theta \sin \varphi_{ij} \mp i c_\theta s_\theta [1 - \cos \varphi_{ij}], \quad (2.81)$$

and Fourier transforming to momentum space, we obtain

$$H_{1\text{mag}}^{1\text{pho}} = \sum_{\mathbf{k}} \Gamma_{\mathbf{k}}^{Xb} \cdot \left(\mathbf{X}_{-\mathbf{k}} b_{\mathbf{k}} + \mathbf{X}_{\mathbf{k}} b_{\mathbf{k}}^\dagger \right), \quad (2.82)$$

with the hybridization vertex given by

$$\Gamma_{\mathbf{k}}^{Xb} = \frac{i}{4} (2S)^{3/2} c_\theta \left[\mathbf{J}_{\mathbf{k},\mathbf{Q}}^{(1+)} + s_\theta \mathbf{J}_{\mathbf{k},\mathbf{Q}}^{(1-)} \right]. \quad (2.83)$$

Here we have defined

$$\mathbf{J}_{\mathbf{k},\mathbf{Q}}^{(1+)} = \mathbf{J}_{\mathbf{Q}}^{(1)} - \frac{\mathbf{J}_{\mathbf{k}+\mathbf{Q}}^{(1)} - \mathbf{J}_{\mathbf{k}-\mathbf{Q}}^{(1)}}{2}, \quad (2.84a)$$

$$\mathbf{J}_{\mathbf{k},\mathbf{Q}}^{(1-)} = \mathbf{J}_{\mathbf{k}}^{(1)} - \frac{\mathbf{J}_{\mathbf{k}+\mathbf{Q}}^{(1)} + \mathbf{J}_{\mathbf{k}-\mathbf{Q}}^{(1)}}{2}. \quad (2.84b)$$

For fixed \mathbf{Q} the functions $\mathbf{J}_{\mathbf{k},\mathbf{Q}}^{(1\pm)}$ have the symmetries

$$\mathbf{J}_{-\mathbf{k},\mathbf{Q}}^{(1\pm)} = \pm \mathbf{J}_{\mathbf{k},\mathbf{Q}}^{(1\pm)}. \quad (2.85)$$

The contribution (2.82) to the Hamiltonian describes the hybridization between magnon and phonon modes. Note that for finite \mathbf{Q} the relevant coupling $\Gamma_{\mathbf{k}}^{Xb}$ vanishes linearly in \mathbf{k} for $\mathbf{k} \rightarrow 0$. As it will be discussed in Sec. III A, the hybridization term $H_{1\text{mag}}^{1\text{pho}}$ gives rise to an additional renormalization of the phonon velocities which has the same order of magnitude as the renormalization due to the contribution $\Sigma_0^{\text{pho}}(\mathbf{k}, \lambda)$ arising from the classical spin background given in Eq. (2.77).

Note that the vertex $\Gamma_{\mathbf{k}}^{Xb}$ does not have a definite symmetry under $\mathbf{k} \rightarrow -\mathbf{k}$. To obtain a more transparent classification of the vertices, it is useful to express the Holstein–Primakoff bosons $b_{\mathbf{k}}$ in terms of Hermitian operators $\Phi_{\mathbf{k}} = \Phi_{-\mathbf{k}}^\dagger$ and $\Pi_{\mathbf{k}} = \Pi_{-\mathbf{k}}^\dagger$ as follows:^{31,32}

$$b_{\mathbf{k}} = \sqrt{\frac{\Delta_{\mathbf{k}}}{2}} \Phi_{\mathbf{k}} + \frac{i}{\sqrt{2\Delta_{\mathbf{k}}}} \Pi_{\mathbf{k}}, \quad (2.86)$$

$$b_{\mathbf{k}}^\dagger = \sqrt{\frac{\Delta_{\mathbf{k}}}{2}} \Phi_{-\mathbf{k}} - \frac{i}{\sqrt{2\Delta_{\mathbf{k}}}} \Pi_{-\mathbf{k}}, \quad (2.87)$$

where the energy $\Delta_{\mathbf{k}}$ is given by

$$\Delta_{\mathbf{k}} = A_{\mathbf{k}}^+ - B_{\mathbf{k}} = A_{\mathbf{k}}^+ + |B_{\mathbf{k}}|. \quad (2.88)$$

Then our quadratic magnon Hamiltonian (2.43) can be written as

$$H_2 = \frac{1}{2} \sum_{\mathbf{k}} \left\{ \Pi_{-\mathbf{k}} \Pi_{\mathbf{k}} + \epsilon_{\mathbf{k}}^2 \Phi_{-\mathbf{k}} \Phi_{\mathbf{k}} + i A_{\mathbf{k}}^- (\Phi_{-\mathbf{k}} \Pi_{\mathbf{k}} - \Phi_{\mathbf{k}} \Pi_{-\mathbf{k}}) - A_{\mathbf{k}}^+ \right\}, \quad (2.89)$$

while the magnon-phonon hybridization (2.82) reads

$$H_{1\text{mag}}^{\text{1pho}} = \frac{1}{2} \sum_{\mathbf{k}} \left\{ \mathbf{\Gamma}_{\mathbf{k}}^{X\Phi} \cdot (\mathbf{X}_{-\mathbf{k}}\Phi_{\mathbf{k}} + \mathbf{X}_{\mathbf{k}}\Phi_{-\mathbf{k}}) + \mathbf{\Gamma}_{\mathbf{k}}^{X\Pi} \cdot (\mathbf{X}_{-\mathbf{k}}\Pi_{\mathbf{k}} - \mathbf{X}_{\mathbf{k}}\Pi_{-\mathbf{k}}) \right\}, \quad (2.90)$$

where the vertex $\mathbf{\Gamma}_{\mathbf{k}}^{X\Phi}$ describing the coupling of the phonon coordinates to the generalized magnon coordinates $\Phi_{\mathbf{k}}$ is an even function of \mathbf{k} , while the corresponding vertex $\mathbf{\Gamma}_{\mathbf{k}}^{X\Pi}$ which couples the phonon coordinates to the magnon momenta is odd in \mathbf{k} :

$$\mathbf{\Gamma}_{\mathbf{k}}^{X\Phi} = \sqrt{\frac{\Delta_{\mathbf{k}}}{2}} [\mathbf{\Gamma}_{\mathbf{k}}^{Xb} + \mathbf{\Gamma}_{-\mathbf{k}}^{Xb}] = \mathbf{\Gamma}_{-\mathbf{k}}^{X\Phi}, \quad (2.91a)$$

$$\mathbf{\Gamma}_{\mathbf{k}}^{X\Pi} = \frac{i}{\sqrt{2\Delta_{\mathbf{k}}}} [\mathbf{\Gamma}_{\mathbf{k}}^{Xb} - \mathbf{\Gamma}_{-\mathbf{k}}^{Xb}] = -\mathbf{\Gamma}_{-\mathbf{k}}^{X\Pi}. \quad (2.91b)$$

In principle, the complete quadratic part $H_2 + H^{\text{pho}} + H_0^{\text{2pho}} + H_{1\text{mag}}^{\text{1pho}}$ of the magnon-phonon Hamiltonian can be diagonalized by means of a canonical transformation.³³ But due to the absence of inversion symmetry of the magnon dispersion $E_{\mathbf{k}}$ the explicit construction of this transformation seems to be a rather complicated mathematical problem which we have not attempted to solve. Fortunately, the renormalized phonon spectrum can be obtained in a straightforward manner at this level of approximation by integrating in the path integral formulation of the theory over the magnon field. As will be shown in Sec. III A, the phonon spectrum can then be directly obtained from the inverse phonon propagator appearing in the resulting Gaussian effective action for the phonon field.

4. One-phonon two-magnon interaction

The part of the spin-phonon Hamiltonian involving one phonon and two magnon operators is

$$H_{2\text{mag}}^{\text{1pho}} = \frac{S}{2} \sum_{ij} U_{ij}^{(1)} \left\{ -\hat{\mathbf{m}}_i \cdot \hat{\mathbf{m}}_j (n_i + n_j) + \frac{1}{2} [(e_i^+ \cdot e_j^-) b_i^\dagger b_j + (e_i^- \cdot e_j^+) b_i b_j^\dagger] + (e_i^+ \cdot e_j^+) b_i^\dagger b_j^\dagger + (e_i^- \cdot e_j^-) b_i b_j \right\}. \quad (2.92)$$

Using Eqs. (2.16–2.18) to calculate the relevant scalar products of the basis vectors, we obtain after Fourier transformation to momentum space,

$$H_{2\text{mag}}^{\text{1pho}} = \frac{1}{\sqrt{N}} \sum_{\mathbf{k}\mathbf{k}'} \left[\mathbf{\Gamma}_{\mathbf{k},\mathbf{k}'}^{b^\dagger b} \cdot \mathbf{X}_{\mathbf{k}-\mathbf{k}'} b_{\mathbf{k}}^\dagger b_{\mathbf{k}'} + \frac{1}{2!} \left(\mathbf{\Gamma}_{\mathbf{k},\mathbf{k}'}^{b^\dagger b^\dagger} \cdot \mathbf{X}_{\mathbf{k}+\mathbf{k}'} b_{\mathbf{k}}^\dagger b_{\mathbf{k}'}^\dagger + \mathbf{\Gamma}_{\mathbf{k},\mathbf{k}'}^{bb} \cdot \mathbf{X}_{-\mathbf{k}-\mathbf{k}'} b_{\mathbf{k}} b_{\mathbf{k}'} \right) \right], \quad (2.93)$$

where the coupling functions are

$$\mathbf{\Gamma}_{\mathbf{k},\mathbf{k}'}^{b^\dagger b} = \frac{S}{2} \left\{ (2s_\theta^2 - c_\theta^2) (\mathbf{J}_{\mathbf{k},\mathbf{Q}}^{(1-)} - \mathbf{J}_{\mathbf{k}',\mathbf{Q}}^{(1-)}) + 2 \left[\mathbf{J}_{\mathbf{k}-\mathbf{k}'}^{(1)} - (\mathbf{J}_{\mathbf{k}}^{(1)} - \mathbf{J}_{\mathbf{k}'}^{(1)}) \right] - 2c_\theta^2 \left[\mathbf{J}_{\mathbf{k}-\mathbf{k}',\mathbf{Q}}^{(1-)} - (\mathbf{J}_{\mathbf{k},\mathbf{Q}}^{(1-)} - \mathbf{J}_{\mathbf{k}',\mathbf{Q}}^{(1-)}) \right] + 2s_\theta (\mathbf{J}_{\mathbf{k},\mathbf{Q}}^{(1+)} - \mathbf{J}_{\mathbf{k}',\mathbf{Q}}^{(1+)}) \right\}, \quad (2.94)$$

$$\mathbf{\Gamma}_{\mathbf{k},\mathbf{k}'}^{b^\dagger b^\dagger} = -\mathbf{\Gamma}_{\mathbf{k},\mathbf{k}'}^{bb} = \frac{S}{2} c_\theta^2 \left[\mathbf{J}_{\mathbf{k},\mathbf{Q}}^{(1-)} + \mathbf{J}_{\mathbf{k}',\mathbf{Q}}^{(1-)} \right]. \quad (2.95)$$

Since the Fourier transform $\mathbf{J}_{\mathbf{k}}^{(1)}$ of the derivative of the exchange coupling is purely imaginary, this is also true for the above vertex functions $\mathbf{\Gamma}_{\mathbf{k},\mathbf{k}'}^{b^\dagger b}$, $\mathbf{\Gamma}_{\mathbf{k},\mathbf{k}'}^{b^\dagger b^\dagger}$ and $\mathbf{\Gamma}_{\mathbf{k},\mathbf{k}'}^{bb}$. Note also that the normal vertex $\mathbf{\Gamma}_{\mathbf{k},\mathbf{k}'}^{b^\dagger b}$ is antisymmetric while the anomalous vertices $\mathbf{\Gamma}_{\mathbf{k},\mathbf{k}'}^{b^\dagger b^\dagger}$ and $\mathbf{\Gamma}_{\mathbf{k},\mathbf{k}'}^{bb}$ are symmetric under $\mathbf{k} \leftrightarrow \mathbf{k}'$. Keeping in mind that these vertices are purely imaginary, one easily verifies the following relations,

$$\mathbf{\Gamma}_{\mathbf{k},\mathbf{k}'}^{b^\dagger b} = -\mathbf{\Gamma}_{\mathbf{k}',\mathbf{k}}^{b^\dagger b} = (\mathbf{\Gamma}_{\mathbf{k}',\mathbf{k}}^{b^\dagger b})^*, \quad (2.96a)$$

$$\mathbf{\Gamma}_{\mathbf{k},\mathbf{k}'}^{b^\dagger b^\dagger} = \mathbf{\Gamma}_{\mathbf{k}',\mathbf{k}}^{b^\dagger b^\dagger} = -\mathbf{\Gamma}_{\mathbf{k}',\mathbf{k}}^{bb} = (\mathbf{\Gamma}_{\mathbf{k}',\mathbf{k}}^{bb})^*, \quad (2.96b)$$

$$\mathbf{\Gamma}_{\mathbf{k},\mathbf{k}'}^{bb} = \mathbf{\Gamma}_{\mathbf{k}',\mathbf{k}}^{bb} = -\mathbf{\Gamma}_{\mathbf{k}',\mathbf{k}}^{b^\dagger b^\dagger} = (\mathbf{\Gamma}_{\mathbf{k}',\mathbf{k}}^{b^\dagger b^\dagger})^*. \quad (2.96c)$$

Of particular interest is the leading behavior of the above magnon-phonon vertices for small \mathbf{k} and \mathbf{k}' ,

$$\mathbf{\Gamma}_{\mathbf{k},\mathbf{k}'}^{b^\dagger b} = \frac{S}{2} \left\{ (2s_\theta^2 - c_\theta^2) [(\mathbf{k} - \mathbf{k}') \cdot \nabla_{\mathbf{Q}}] [\mathbf{J}_{\mathbf{Q}}^{(1)} \Big|_{\mathbf{Q}=0} - \mathbf{J}_{\mathbf{Q}}^{(1)}] - s_\theta [(\mathbf{k} \cdot \nabla_{\mathbf{Q}})^2 - (\mathbf{k}' \cdot \nabla_{\mathbf{Q}})^2] \mathbf{J}_{\mathbf{Q}}^{(1)} \right\} + \mathcal{O}(\mathbf{k}^3), \quad (2.97)$$

$$\mathbf{\Gamma}_{\mathbf{k},\mathbf{k}'}^{b^\dagger b^\dagger} = \frac{S}{2} c_\theta^2 [(\mathbf{k} + \mathbf{k}') \cdot \nabla_{\mathbf{Q}}] [\mathbf{J}_{\mathbf{Q}}^{(1)} \Big|_{\mathbf{Q}=0} - \mathbf{J}_{\mathbf{Q}}^{(1)}] + \mathcal{O}(\mathbf{k}^3). \quad (2.98)$$

It turns out that $H_{2\text{mag}}^{\text{1pho}}$ in Eq. (2.93) is not the only part of the Hamiltonian describing the coupling of a single phonon to two magnon operators. The reason is that due to the magnon-phonon hybridization discussed in Sec. II C 3 the Holstein–Primakoff bosons are a linear combination of true magnon operators and phonon operators. In principle, the proper linear combination can be obtained by diagonalizing the quadratic magnon-phonon Hamiltonian $H_2 + H^{\text{pho}} + H_0^{\text{2pho}} + H_{1\text{mag}}^{\text{1pho}}$ by means of a canonical transformation. Although the construction of such a transformation is in principle possible,³³ for our purposes it is fortunately not necessary to explicitly solve this complicated algebraic problem. The reason is that at long wavelengths and to the order in the small parameter $1/S$ consistent with Eq. (2.92), the proper magnon operators $\tilde{b}_{\mathbf{k}}$ can be determined from the requirement that in the quadratic part of the magnon-phonon Hamiltonian

$H_2 + H^{\text{pho}} + H_0^{2\text{pho}} + H_{1\text{mag}}^{1\text{pho}}$ there should be no terms describing the coupling of the phonon coordinates $\mathbf{X}_{\mathbf{k}}$ to the generalized magnon momenta $\Pi_{\mathbf{k}}$, as in the second line of Eq. (2.90). It is then easy to show that the proper magnon operators $\tilde{b}_{\mathbf{k}}$ are related to the original Holstein–Primakoff magnons $b_{\mathbf{k}}$ via the phonon-dependent shift transformation

$$b_{\mathbf{k}} = \tilde{b}_{\mathbf{k}} + \boldsymbol{\lambda}_{\mathbf{k}} \cdot \mathbf{X}_{\mathbf{k}}, \quad (2.99)$$

where

$$\boldsymbol{\lambda}_{\mathbf{k}} = \frac{i}{\sqrt{2\Delta_{\mathbf{k}}}} \boldsymbol{\Gamma}_{\mathbf{k}}^{X\Pi} \quad (2.100)$$

depends on the antisymmetric vertex $\boldsymbol{\Gamma}_{\mathbf{k}}^{X\Pi}$ defined in Eq. (2.91b). If we now substitute the transformation (2.99) into the part H_3 of the pure magnon Hamiltonian involving three powers of the Holstein–Primakoff bosons given in Eq. (2.56), we generate (among other terms) an additional contribution to the one-phonon two-magnon interaction, which involves the same power of S as $H_{2\text{mag}}^{1\text{pho}}$ in Eq. (2.92) and therefore should be taken into account on equal footing with $H_{2\text{mag}}^{1\text{pho}}$. Fortunately, this contribution can be absorbed via a simple redefinition of the vertices in Eq. (2.93),

$$\tilde{\boldsymbol{\Gamma}}_{\mathbf{k},\mathbf{k}'}^{b^\dagger b} = \boldsymbol{\Gamma}_{\mathbf{k},\mathbf{k}'}^{b^\dagger b} + \delta\boldsymbol{\Gamma}_{\mathbf{k},\mathbf{k}'}^{b^\dagger b}, \quad (2.101a)$$

$$\tilde{\boldsymbol{\Gamma}}_{\mathbf{k},\mathbf{k}'}^{b^\dagger b^\dagger} = \boldsymbol{\Gamma}_{\mathbf{k},\mathbf{k}'}^{b^\dagger b^\dagger} + \delta\boldsymbol{\Gamma}_{\mathbf{k},\mathbf{k}'}^{b^\dagger b^\dagger}, \quad (2.101b)$$

$$\tilde{\boldsymbol{\Gamma}}_{\mathbf{k},\mathbf{k}'}^{bb} = \boldsymbol{\Gamma}_{\mathbf{k},\mathbf{k}'}^{bb} + \delta\boldsymbol{\Gamma}_{\mathbf{k},\mathbf{k}'}^{bb}, \quad (2.101c)$$

where the correction terms due to magnon-phonon hybridization are

$$\begin{aligned} \delta\boldsymbol{\Gamma}_{\mathbf{k},\mathbf{k}'}^{b^\dagger b} &= \boldsymbol{\Gamma}_3^{b^\dagger b^\dagger b}(\mathbf{k} - \mathbf{k}', -\mathbf{k}; \mathbf{k}') \boldsymbol{\lambda}_{\mathbf{k}' - \mathbf{k}} \\ &\quad + \boldsymbol{\Gamma}_3^{b^\dagger bb}(-\mathbf{k}; \mathbf{k}', \mathbf{k} - \mathbf{k}') \boldsymbol{\lambda}_{\mathbf{k} - \mathbf{k}'}, \end{aligned} \quad (2.102a)$$

$$\delta\boldsymbol{\Gamma}_{\mathbf{k},\mathbf{k}'}^{b^\dagger b^\dagger} = \boldsymbol{\Gamma}_3^{b^\dagger b^\dagger b}(-\mathbf{k}, -\mathbf{k}'; \mathbf{k} + \mathbf{k}') \boldsymbol{\lambda}_{\mathbf{k} + \mathbf{k}'}, \quad (2.102b)$$

$$\delta\boldsymbol{\Gamma}_{\mathbf{k},\mathbf{k}'}^{bb} = \boldsymbol{\Gamma}_3^{b^\dagger bb}(-\mathbf{k} - \mathbf{k}'; \mathbf{k}, \mathbf{k}') \boldsymbol{\lambda}_{\mathbf{k} + \mathbf{k}'}. \quad (2.102c)$$

The effective one-phonon two-magnon Hamiltonian $\tilde{H}_{2\text{mag}}^{1\text{pho}}$ can then be obtained from $H_{2\text{mag}}^{1\text{pho}}$ in Eq. (2.93) by substituting the bare vertices by the shifted ones, $\boldsymbol{\Gamma}_{\mathbf{k},\mathbf{k}'}^{b^\dagger b} \rightarrow \tilde{\boldsymbol{\Gamma}}_{\mathbf{k},\mathbf{k}'}^{b^\dagger b}$, $\boldsymbol{\Gamma}_{\mathbf{k},\mathbf{k}'}^{b^\dagger b^\dagger} \rightarrow \tilde{\boldsymbol{\Gamma}}_{\mathbf{k},\mathbf{k}'}^{b^\dagger b^\dagger}$, and $\boldsymbol{\Gamma}_{\mathbf{k},\mathbf{k}'}^{bb} \rightarrow \tilde{\boldsymbol{\Gamma}}_{\mathbf{k},\mathbf{k}'}^{bb}$. Using the fact that according to Eqs. (2.57a–2.59) at long wavelengths the three-magnon vertices can be approximated by

$$\begin{aligned} \boldsymbol{\Gamma}_3^{b^\dagger b^\dagger b}(\mathbf{k}_1, \mathbf{k}_2; \mathbf{k}_3) &= -\boldsymbol{\Gamma}_3^{b^\dagger bb}(-\mathbf{k}_3, -\mathbf{k}_2; -\mathbf{k}_1) \\ &= -c_\theta s_\theta \frac{\sqrt{2S} h_c}{i S} + \mathcal{O}(\mathbf{k}^2), \end{aligned} \quad (2.103)$$

we obtain for the shifts of the one-phonon two-magnon vertices due to magnon-phonon hybridization at long

wavelengths,

$$\begin{aligned} \delta\boldsymbol{\Gamma}_{\mathbf{k},\mathbf{k}'}^{b^\dagger b} &= -2Ss_\theta^2 [(\mathbf{k} - \mathbf{k}') \cdot \nabla_{\mathbf{Q}}] [J_{\mathbf{Q}}^{(1)} \Big|_{\mathbf{Q}=0} - J_{\mathbf{Q}}^{(1)}] \\ &\quad + \mathcal{O}(\mathbf{k}^3), \end{aligned} \quad (2.104)$$

$$\begin{aligned} \delta\boldsymbol{\Gamma}_{\mathbf{k},\mathbf{k}'}^{b^\dagger b^\dagger} &= Ss_\theta^2 [(\mathbf{k} + \mathbf{k}') \cdot \nabla_{\mathbf{Q}}] [J_{\mathbf{Q}}^{(1)} \Big|_{\mathbf{Q}=0} - J_{\mathbf{Q}}^{(1)}] \\ &\quad + \mathcal{O}(\mathbf{k}^3). \end{aligned} \quad (2.105)$$

Combining these expressions with the long-wavelength limits of the corresponding bare vertices given in Eqs. (2.97, 2.98), we find that the proper one-phonon two-magnon vertices are in the long-wavelength limit given by

$$\begin{aligned} \tilde{\boldsymbol{\Gamma}}_{\mathbf{k},\mathbf{k}'}^{b^\dagger b} &= \\ &= -\frac{S}{2} \left\{ (2s_\theta^2 + c_\theta^2) [(\mathbf{k} - \mathbf{k}') \cdot \nabla_{\mathbf{Q}}] [J_{\mathbf{Q}}^{(1)} \Big|_{\mathbf{Q}=0} - J_{\mathbf{Q}}^{(1)}] \right. \\ &\quad \left. + s_\theta [(\mathbf{k} \cdot \nabla_{\mathbf{Q}})^2 - (\mathbf{k}' \cdot \nabla_{\mathbf{Q}})^2] J_{\mathbf{Q}}^{(1)} \right\} + \mathcal{O}(\mathbf{k}^3), \end{aligned} \quad (2.106)$$

$$\begin{aligned} \tilde{\boldsymbol{\Gamma}}_{\mathbf{k},\mathbf{k}'}^{b^\dagger b^\dagger} &= \frac{S}{2} (2s_\theta^2 + c_\theta^2) [(\mathbf{k} + \mathbf{k}') \cdot \nabla_{\mathbf{Q}}] [J_{\mathbf{Q}}^{(1)} \Big|_{\mathbf{Q}=0} - J_{\mathbf{Q}}^{(1)}] \\ &\quad + \mathcal{O}(\mathbf{k}^3). \end{aligned} \quad (2.107)$$

Note that the coefficients of the terms linear in the momenta differ only by a minus sign, which will turn out to be essential to obtain the correct long-wavelength limit of the ultrasonic attenuation rate.

At this point it is convenient to express the effective one-phonon two-magnon Hamiltonian $\tilde{H}_{2\text{mag}}^{1\text{pho}}$ in terms of the Bogoliubov quasiparticle operators $\beta_{\mathbf{k}}$ and $\beta_{\mathbf{k}}^\dagger$ defined in Eq. (2.47). We obtain

$$\begin{aligned} \tilde{H}_{2\text{mag}}^{1\text{pho}} &= \frac{1}{\sqrt{N}} \sum_{\mathbf{k}\mathbf{k}'} \left[\tilde{\boldsymbol{\Gamma}}_{\mathbf{k},\mathbf{k}'}^{\beta^\dagger \beta} \cdot \mathbf{X}_{\mathbf{k}-\mathbf{k}'} \beta_{\mathbf{k}}^\dagger \beta_{\mathbf{k}'} \right. \\ &\quad \left. + \frac{1}{2!} \left(\tilde{\boldsymbol{\Gamma}}_{\mathbf{k},\mathbf{k}'}^{\beta^\dagger \beta^\dagger} \cdot \mathbf{X}_{\mathbf{k}+\mathbf{k}'} \beta_{\mathbf{k}}^\dagger \beta_{\mathbf{k}'}^\dagger + \tilde{\boldsymbol{\Gamma}}_{\mathbf{k},\mathbf{k}'}^{\beta\beta} \cdot \mathbf{X}_{-\mathbf{k}-\mathbf{k}'} \beta_{\mathbf{k}} \beta_{\mathbf{k}'} \right) \right], \end{aligned} \quad (2.108)$$

where the vertices are given by

$$\begin{aligned} \tilde{\boldsymbol{\Gamma}}_{\mathbf{k},\mathbf{k}'}^{\beta^\dagger \beta} &= u_{\mathbf{k}} u_{\mathbf{k}'} \tilde{\boldsymbol{\Gamma}}_{\mathbf{k},\mathbf{k}'}^{b^\dagger b} - v_{\mathbf{k}} v_{\mathbf{k}'} \tilde{\boldsymbol{\Gamma}}_{-\mathbf{k}, -\mathbf{k}'}^{b^\dagger b} \\ &\quad - u_{\mathbf{k}} v_{\mathbf{k}'} \tilde{\boldsymbol{\Gamma}}_{\mathbf{k}, -\mathbf{k}'}^{b^\dagger b^\dagger} - v_{\mathbf{k}} u_{\mathbf{k}'} \tilde{\boldsymbol{\Gamma}}_{-\mathbf{k}, \mathbf{k}'}^{bb}, \end{aligned} \quad (2.109a)$$

$$\begin{aligned} \tilde{\boldsymbol{\Gamma}}_{\mathbf{k},\mathbf{k}'}^{\beta^\dagger \beta^\dagger} &= u_{\mathbf{k}} u_{\mathbf{k}'} \tilde{\boldsymbol{\Gamma}}_{\mathbf{k},\mathbf{k}'}^{b^\dagger b^\dagger} + v_{\mathbf{k}} v_{\mathbf{k}'} \tilde{\boldsymbol{\Gamma}}_{-\mathbf{k}, -\mathbf{k}'}^{bb} \\ &\quad - u_{\mathbf{k}} v_{\mathbf{k}'} \tilde{\boldsymbol{\Gamma}}_{\mathbf{k}, -\mathbf{k}'}^{b^\dagger b} + v_{\mathbf{k}} u_{\mathbf{k}'} \tilde{\boldsymbol{\Gamma}}_{-\mathbf{k}, \mathbf{k}'}^{b^\dagger b}, \end{aligned} \quad (2.109b)$$

$$\begin{aligned} \tilde{\boldsymbol{\Gamma}}_{\mathbf{k},\mathbf{k}'}^{\beta\beta} &= u_{\mathbf{k}} u_{\mathbf{k}'} \tilde{\boldsymbol{\Gamma}}_{\mathbf{k},\mathbf{k}'}^{bb} + v_{\mathbf{k}} v_{\mathbf{k}'} \tilde{\boldsymbol{\Gamma}}_{-\mathbf{k}, -\mathbf{k}'}^{b^\dagger b^\dagger} \\ &\quad + u_{\mathbf{k}} v_{\mathbf{k}'} \tilde{\boldsymbol{\Gamma}}_{\mathbf{k}, -\mathbf{k}'}^{b^\dagger b} - v_{\mathbf{k}} u_{\mathbf{k}'} \tilde{\boldsymbol{\Gamma}}_{-\mathbf{k}, \mathbf{k}'}^{b^\dagger b}. \end{aligned} \quad (2.109c)$$

As will be shown in Sec. IIIB, at zero temperature the ultrasonic attenuation rate is determined by the anomalous vertex $\tilde{\boldsymbol{\Gamma}}_{\mathbf{k},\mathbf{k}'}^{\beta^\dagger \beta^\dagger}$, whose long-wavelength limit is explic-

itly given by

$$\begin{aligned} \tilde{\Gamma}_{\mathbf{k}, \mathbf{k}'}^{\beta^\dagger \beta^\dagger} &= \frac{S}{2} \left\{ \right. \\ &\left. \left(\frac{2s_\theta^2}{c_\theta^2} + 1 \right) \sqrt{\frac{\epsilon_{\mathbf{k}} \epsilon_{\mathbf{k}'}}{h_c^2}} [(\mathbf{k} + \mathbf{k}') \cdot \nabla_{\mathbf{Q}}] [\mathbf{J}_{\mathbf{Q}}^{(1)}]_{\mathbf{Q}=0} - \mathbf{J}_{\mathbf{Q}}^{(1)} \right\} \\ &+ \frac{s_\theta}{2} \frac{\epsilon_{\mathbf{k}} - \epsilon_{\mathbf{k}'}}{\sqrt{\epsilon_{\mathbf{k}} \epsilon_{\mathbf{k}'}}} [(\mathbf{k} \cdot \nabla_{\mathbf{Q}})^2 - (\mathbf{k}' \cdot \nabla_{\mathbf{Q}})^2] \mathbf{J}_{\mathbf{Q}}^{(1)} \left. \right\} + \mathcal{O}(\mathbf{k}^3). \end{aligned} \quad (2.110)$$

III. PHONON SELF-ENERGY DUE TO MAGNON-PHONON INTERACTIONS

A. Elastic constants

The elastic constants are directly related to the velocities of the acoustic phonons which can be determined experimentally with high accuracy.²⁰ Although the spin-phonon coupling is expected to be small, its influence on the phonon properties is visible in the magnetic-field dependence of the elastic constants. The leading contributions to the shift in the elastic constants is already contained in the quadratic magnon-phonon Hamiltonian $H_2 + H^{\text{pho}} + H_0^{2\text{pho}} + H_{1\text{mag}}^{1\text{pho}}$. The phonon self-energy $\Sigma_0^{\text{pho}}(\mathbf{k}, \lambda)$ given in Eq. (2.77) which is due to the coupling of the phonons to the classical spin background renormalizes the phonon frequencies according to $\omega_{\mathbf{k}\lambda}^2 \rightarrow \omega_{\mathbf{k}\lambda}^2 + \Sigma_0^{\text{pho}}(\mathbf{k}, \lambda)$. The self-energy correction leads to the following relative shift of the phonon velocities,

$$\frac{(\Delta c_\lambda)_0}{c_\lambda} = \sqrt{1 - \lim_{|\mathbf{k}| \rightarrow 0} \frac{\Sigma_0^{\text{pho}}(\mathbf{k}, \lambda)}{\omega_{\mathbf{k}\lambda}^2}} - 1. \quad (3.1)$$

An additional renormalization of the phonon velocities arises from the magnon-phonon hybridization in Eq. (2.82). To calculate this contribution, we note that the phonons couple to the magnons only via the combination $\mathbf{X}_{\mathbf{k}} = \sum_\lambda X_{\mathbf{k}\lambda} \mathbf{e}_{\mathbf{k}\lambda}$ so that it is convenient to describe the phonon dynamics within an effective Lagrangian which is obtained by integrating over the canonical phonon momenta $P_{\mathbf{k}\lambda}$ in the phase space functional integral representation of the theory.³² To leading order for large S we may truncate the effective Euclidean action at the quadratic order in the fluctuations,

$$S[\mathbf{X}, \bar{\beta}, \beta] \approx S^{2\text{pho}}[\mathbf{X}] + S_{2\text{mag}}[\bar{\beta}, \beta] + S_{1\text{mag}}^{1\text{pho}}[\mathbf{X}, \bar{\beta}, \beta], \quad (3.2)$$

where the Gaussian actions $S^{2\text{pho}}[\mathbf{X}]$ and $S_{2\text{mag}}[\bar{\beta}, \beta]$ describe noninteracting phonons and magnons,

$$S^{2\text{pho}}[\mathbf{X}] = \frac{1}{2T} \sum_{K\lambda} M[\omega^2 + \omega_{\mathbf{k}\lambda}^2 + \Sigma_0^{\text{pho}}(\mathbf{k}, \lambda)] \times X_{-K\lambda} X_{K\lambda}, \quad (3.3)$$

$$S_{2\text{mag}}[\bar{\beta}, \beta] = -\frac{1}{T} \sum_K (i\omega - E_{\mathbf{k}}) \bar{\beta}_K \beta_K. \quad (3.4)$$

Here T is the temperature and $K = (i\omega, \mathbf{k})$ is a collective label containing bosonic Matsubara frequencies $i\omega$ and wavevectors \mathbf{k} . The real field $X_{K\lambda}$ represents the Fourier components of the phonon operator $X_{\mathbf{k}\lambda}$, while the complex boson field β_K represents the Fourier components of the magnon operator $\beta_{\mathbf{k}}$. From Eqs. (2.47, 2.82) we see that the magnon-phonon hybridization is represented by the Euclidean action

$$S_{1\text{mag}}^{1\text{pho}}[\mathbf{X}, \bar{\beta}, \beta] = \frac{1}{T} \sum_K \Gamma_{\mathbf{k}}^{X\beta} \cdot (\mathbf{X}_{-K} \beta_K + \mathbf{X}_K \bar{\beta}_K), \quad (3.5)$$

where the hybridization vertex is the following linear combination of the corresponding hybridization vertex $\Gamma_{\mathbf{k}}^{Xb}$ in the Holstein–Primakoff basis given in Eq. (2.83),

$$\Gamma_{\mathbf{k}}^{X\beta} = u_{\mathbf{k}} \Gamma_{\mathbf{k}}^{Xb} - v_{\mathbf{k}} \Gamma_{-\mathbf{k}}^{Xb}. \quad (3.6)$$

The Gaussian integral over the magnon field is now easily carried out, and we obtain for the effective phonon action in Gaussian approximation,

$$\begin{aligned} S_{\text{eff}}^{2\text{pho}}[\mathbf{X}] &= \frac{1}{2T} \sum_{K\lambda\lambda'} \left[\delta_{\lambda,\lambda'} M[\omega^2 + \omega_{\mathbf{k}\lambda}^2 + \Sigma_0^{\text{pho}}(\mathbf{k}, \lambda)] \right. \\ &\left. + \frac{(\Gamma_{\mathbf{k}}^{X\beta} \cdot \mathbf{e}_{\mathbf{k}\lambda})^* (\Gamma_{\mathbf{k}}^{X\beta} \cdot \mathbf{e}_{\mathbf{k}\lambda'})}{i\omega - E_{\mathbf{k}}} \right] X_{-K\lambda} X_{K\lambda'}. \end{aligned} \quad (3.7)$$

For simplicity, we neglect in the sum over the phonon modes the optical phonons and off-diagonal terms $\lambda \neq \lambda'$. In this approximation the magnon-phonon hybridization generates the following phonon self-energy:

$$\Sigma_1^{\text{pho}}(K, \lambda) = \frac{|\Gamma_{\mathbf{k}}^{X\beta} \cdot \mathbf{e}_{\mathbf{k}\lambda}|^2}{M(i\omega - E_{\mathbf{k}})}. \quad (3.8)$$

Combining this with the classical self-energy $\Sigma_0^{\text{pho}}(\mathbf{k}, \lambda)$ given in Eq. (2.77), we conclude that the renormalized phonon dispersion $\tilde{\omega}_{\mathbf{k}\lambda}$ is determined by the real positive root of the cubic equation

$$\begin{aligned} \tilde{\omega}_{\mathbf{k}\lambda}^2 &= \omega_{\mathbf{k}\lambda}^2 + \Sigma_0^{\text{pho}}(\mathbf{k}, \lambda) + \Sigma_1^{\text{pho}}(i\omega \rightarrow \tilde{\omega}_{\mathbf{k}\lambda}, \mathbf{k}, \lambda) \\ &= \omega_{\mathbf{k}\lambda}^2 + \Sigma_0^{\text{pho}}(\mathbf{k}, \lambda) + \frac{|\Gamma_{\mathbf{k}}^{X\beta} \cdot \mathbf{e}_{\mathbf{k}\lambda}|^2}{M(\tilde{\omega}_{\mathbf{k}\lambda} - E_{\mathbf{k}})}. \end{aligned} \quad (3.9)$$

Recall that according to Eq. (2.77) the classical self-energy $\Sigma_0^{\text{pho}}(\mathbf{k}, \lambda)$ is proportional to S^2 . Keeping in mind that according to Eq. (2.83) the hybridization vertex $\Gamma_{\mathbf{k}}^{X\beta}$ is of order $S^{3/2}$ and the denominator in Eq. (3.8) contains one power of $E_{\mathbf{k}} \propto S$, we see that both self-energy contributions on the right-hand side of Eq. (3.9) have the same order of magnitude in a formal $1/S$ -expansion.

Because in the experimentally relevant regime the magnon velocity is small compared with the phonon velocity, the shift in the phonon velocities due to magnon-phonon hybridization can be approximated by

$$\frac{(\Delta c_\lambda)_1}{c_\lambda} = \lim_{|\mathbf{k}| \rightarrow 0} \frac{|\Gamma_{\mathbf{k}}^{X\beta} \cdot \mathbf{e}_{\mathbf{k}\lambda}|^2}{2M\omega_{\mathbf{k}\lambda}^3}. \quad (3.10)$$

Note that this contribution is always positive, i.e. the coupling to the magnons enhances the phonon velocities, which is a simple consequence of the fact that for Cs_2CuCl_4 the magnon velocities are small compared with the phonon velocities. To explicitly take the limit in Eq. (3.10) we need the small-momentum limit of the vertex $\Gamma_{\mathbf{k}}^{X\beta}$. Using Eqs. (2.83) and (3.6) we obtain to leading order

$$\Gamma_{\mathbf{k}}^{X\beta} = \frac{i}{4}(2S)^{3/2}|\mathbf{k}|^{3/2}\sqrt{\frac{v(\hat{\mathbf{k}})}{h_c}}\mathbf{F}^{X\beta}(\hat{\mathbf{k}}), \quad (3.11)$$

where the dimensionless vector $\mathbf{F}^{X\beta}(\hat{\mathbf{k}})$ is given by

$$\mathbf{F}^{X\beta}(\hat{\mathbf{k}}) = s_\theta \mathbf{f}_1^{X\beta}(\hat{\mathbf{k}}) - c_\theta^2 \mathbf{f}_2^{X\beta}(\hat{\mathbf{k}}, \hat{\mathbf{k}}), \quad (3.12)$$

and we introduced the auxiliary vector functions

$$\mathbf{f}_1^{X\beta}(\hat{\mathbf{k}}) = \frac{1}{h_c}(\hat{\mathbf{k}} \cdot \nabla_{\mathbf{Q}}) \left[\mathbf{J}_{\mathbf{Q}}^{(1)} \Big|_{\mathbf{Q}=0} - \mathbf{J}_{\mathbf{Q}}^{(1)} \right], \quad (3.13a)$$

$$\mathbf{f}_2^{X\beta}(\hat{\mathbf{k}}, \hat{\mathbf{k}}') = \frac{1}{2v(\hat{\mathbf{k}})}(\hat{\mathbf{k}} \cdot \nabla_{\mathbf{Q}})(\hat{\mathbf{k}}' \cdot \nabla_{\mathbf{Q}})\mathbf{J}_{\mathbf{Q}}^{(1)}. \quad (3.13b)$$

Here we have approximated the magnon dispersion by its leading long-wavelength limit, $E_{\mathbf{k}} \approx \epsilon_{\mathbf{k}} \approx v(\hat{\mathbf{k}})|\mathbf{k}|$; see Eqs. (2.52) and (2.53). Substituting Eq. (3.12) into Eq. (3.10) we finally obtain

$$\begin{aligned} \frac{(\Delta c_\lambda)_1}{c_\lambda} &= \frac{S^3}{4} \left(\frac{v(\hat{\mathbf{k}})}{c_\lambda} \right) \left(\frac{h_c}{Mc_\lambda^2} \right) |\mathbf{F}^{X\beta}(\hat{\mathbf{k}}) \cdot \mathbf{e}_{\mathbf{k}\lambda}|^2 \\ &= \frac{S^3}{4} \left(\frac{v(\hat{\mathbf{k}})}{c_\lambda} \right) \left(\frac{h_c}{Mc_\lambda^2} \right) \\ &\quad \times |s_\theta \mathbf{f}_1^{X\beta}(\hat{\mathbf{k}}) \cdot \mathbf{e}_{\mathbf{k}\lambda} - c_\theta^2 \mathbf{f}_2^{X\beta}(\hat{\mathbf{k}}, \hat{\mathbf{k}}) \cdot \mathbf{e}_{\mathbf{k}\lambda}|^2. \end{aligned} \quad (3.14)$$

Formally, this is the leading-order contribution in the small parameters $v(\hat{\mathbf{k}})/c_\lambda$ and $h_c/(Mc_\lambda^2)$. Note that the magnetic-field dependence of the vertex (3.12) is hidden in the canting angle θ , which we approximate by its classical value (2.36). Adding the classical and the hybridization contributions, we finally obtain for the total velocity shift,

$$\frac{\Delta c_\lambda}{c_\lambda} = \frac{(\Delta c_\lambda)_0 + (\Delta c_\lambda)_1}{c_\lambda}. \quad (3.15)$$

Depending on the polarization vector $\mathbf{e}_{\mathbf{k}\lambda}$ of the phonon and on the structure of the first-derivative vector $\mathbf{J}_{\mathbf{k}}^{(1)}$ and the second derivative tensor $\mathbf{J}_{\mathbf{k}}^{(2)}$, either the first or the second contribution on the right-hand side of Eq. (3.15) can dominate. In Sec. IV we shall explicitly evaluate Eq. (3.15) for the specific parameters of Cs_2CuCl_4 and compare our results with experiments.

B. Ultrasonic attenuation

To obtain the magnetic-field dependence of the ultrasonic attenuation rate, we should calculate the damping

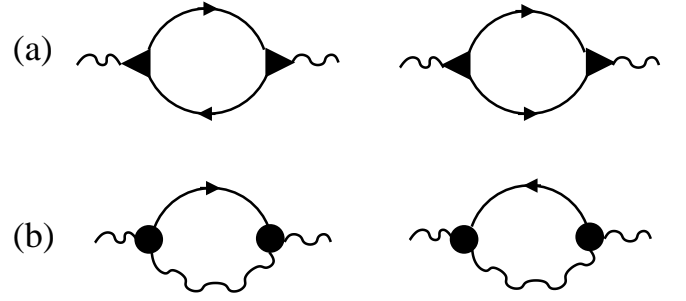


FIG. 5. These Feynman diagrams represent contributions to the phonon self-energy which determine the ultrasonic attenuation rate to leading order in the large- S expansion. (a) One-phonon two-magnon processes. (b) Two-phonon one-magnon processes. Wavy lines represent the phonon Green's functions $G^{\text{pho}}(K\lambda)$, solid arrows represent the magnon propagators $G_{\text{mag}}(K)$, black triangles represent the shifted one-phonon two-magnon vertices defined in Eqs. (2.109a–2.109c), while black circles represent the two-phonon one-magnon vertices defined in Eqs. (A.6, A.7). Both processes lead to an attenuation rate proportional to k^4 at long wavelengths. The processes (a) exhibit a stronger dependence on the external magnetic field and dominate if the magnon velocities are small compared with the phonon velocities.

of the phonons due to the coupling to the magnon system. In principle, the attenuation rate can be obtained using Fermi's golden rule. Due to the rather complicated matrix elements of the relevant interaction vertices, we find it more convenient to use a many-body approach where the damping rate is obtained from the imaginary part of the phonon self-energy. The lowest-order interaction processes leading to phonon damping are shown diagrammatically in Fig. 5. It turns out that only the processes in Fig. 5(a) involving two magnons in the intermediate lead to a strong magnetic-field dependence of the ultrasonic attenuation rate, so that we shall focus here on these processes. In the appendix we shall show that for Cs_2CuCl_4 where the magnon velocities are small compared with the phonon velocities the other processes in Fig. 5(b) involving one magnon and one phonon in the intermediate state can indeed be neglected. To obtain the contribution of the processes shown in Fig. 5(a) to the ultrasonic attenuation rate, it is sufficient to retain only the effective one-phonon two-magnon interaction process in our coupled magnon-phonon action. We thus approximate

$$S[\mathbf{X}, \bar{\beta}, \beta] = S^{\text{2pho}}[\mathbf{X}] + S_{2\text{mag}}[\bar{\beta}, \beta] + \tilde{S}_{2\text{mag}}^{\text{1pho}}[\mathbf{X}, \bar{\beta}, \beta], \quad (3.16)$$

where the Gaussian parts $S^{\text{2pho}}[\mathbf{X}]$ and $S_{2\text{mag}}[\bar{\beta}, \beta]$ are given in Eqs. (3.3, 3.4), while the effective magnon-

phonon interaction is

$$\begin{aligned} \tilde{S}_{2\text{mag}}^{\text{1pho}}[\mathbf{X}, \bar{\beta}, \beta] &= \frac{1}{\sqrt{NT}} \sum_{K, K'} \left[\tilde{\Gamma}_{\mathbf{k}, \mathbf{k}'}^{\beta^\dagger \beta} \cdot \mathbf{X}_{K-K'} \bar{\beta}_K \beta_{K'} \right. \\ &\left. + \frac{1}{2!} \left(\tilde{\Gamma}_{\mathbf{k}, \mathbf{k}'}^{\beta^\dagger \beta^\dagger} \cdot \mathbf{X}_{K+K'} \bar{\beta}_K \bar{\beta}_{K'} + \tilde{\Gamma}_{\mathbf{k}, \mathbf{k}'}^{\beta \beta} \cdot \mathbf{X}_{-K-K'} \beta_K \beta_{K'} \right) \right], \end{aligned} \quad (3.17)$$

which corresponds to the effective one-phonon two-magnon Hamiltonian $\tilde{H}_{2\text{mag}}^{\text{1pho}}$ defined in Eq. (2.108). Note that the vertices in this expression take the magnon-phonon hybridization into account. The phonon self-energy $\Sigma^{\text{pho}}(K\lambda)$ and the magnon self-energy $\Sigma_{\text{mag}}(K)$ are defined in terms of the corresponding Green's functions:

$$G^{\text{pho}}(K\lambda) = \frac{M}{T} \langle X_{-K\lambda} X_{K\lambda} \rangle = \frac{1}{\omega^2 + \omega_{\mathbf{k}\lambda}^2 + \Sigma^{\text{pho}}(K\lambda)}, \quad (3.18)$$

$$G_{\text{mag}}(K) = -\frac{1}{T} \langle \bar{\beta}_K \beta_K \rangle = \frac{1}{i\omega - E_{\mathbf{k}} - \Sigma_{\text{mag}}(K)}. \quad (3.19)$$

The diagrams shown in Fig. 5 (a) give rise to the following contribution to the phonon self-energy,

$$\begin{aligned} \Sigma_2^{\text{pho}}(K\lambda) &= -\frac{T}{N} \sum_{K'} \left[\right. \\ &\quad \frac{|\tilde{\Gamma}_{\mathbf{k}', \mathbf{k}'-\mathbf{k}}^{\beta^\dagger \beta} \cdot \mathbf{e}_{\mathbf{k}\lambda}|^2}{2M} G_{\text{mag}}(K') G_{\text{mag}}(K' - K) \\ &\quad \left. + \frac{|\tilde{\Gamma}_{\mathbf{k}', \mathbf{k}-\mathbf{k}'}^{\beta^\dagger \beta^\dagger} \cdot \mathbf{e}_{\mathbf{k}\lambda}|^2}{2M} G_{\text{mag}}(K') G_{\text{mag}}(K - K') \right] \\ &\quad + (K \rightarrow -K). \end{aligned} \quad (3.20)$$

Neglecting self-energy corrections to the magnon propagators, the frequency summation can be easily carried out,

$$\begin{aligned} \Sigma_2^{\text{pho}}(K\lambda) &= \\ &\quad -\frac{1}{N} \sum_{\mathbf{k}'} \left[\frac{|\tilde{\Gamma}_{\mathbf{k}', \mathbf{k}'-\mathbf{k}}^{\beta^\dagger \beta} \cdot \mathbf{e}_{\mathbf{k}\lambda}|^2}{2M} \frac{n(E_{\mathbf{k}'}) - n(E_{\mathbf{k}'-\mathbf{k}})}{i\omega - E_{\mathbf{k}'} + E_{\mathbf{k}'-\mathbf{k}}} \right. \\ &\quad \left. + \frac{|\tilde{\Gamma}_{\mathbf{k}', \mathbf{k}-\mathbf{k}'}^{\beta^\dagger \beta^\dagger} \cdot \mathbf{e}_{\mathbf{k}\lambda}|^2}{2M} \frac{n(E_{\mathbf{k}'}) + n(E_{\mathbf{k}-\mathbf{k}'}) + 1}{-i\omega + E_{\mathbf{k}'} + E_{\mathbf{k}-\mathbf{k}'}} \right] \\ &\quad + (K \rightarrow -K), \end{aligned} \quad (3.21)$$

where $n(E) = 1/(e^{E/T} - 1)$ is the Bose function. To calculate the phonon damping, we analytically continue this expression to the real frequency axis, $i\omega \rightarrow \omega + i0$, and take the imaginary part. We obtain

$$\begin{aligned} \text{Im}\Sigma_2^{\text{pho}}(\omega + i0, \mathbf{k}, \lambda) &= -[1 - e^{-\omega/T}] \frac{\pi}{N} \sum_{\mathbf{k}'} \left[\frac{|\tilde{\Gamma}_{\mathbf{k}', \mathbf{k}'-\mathbf{k}}^{\beta^\dagger \beta} \cdot \mathbf{e}_{\mathbf{k}\lambda}|^2}{2M} \delta(\omega - E_{\mathbf{k}'} + E_{\mathbf{k}'-\mathbf{k}}) [1 + n(E_{\mathbf{k}'})] n(E_{\mathbf{k}'-\mathbf{k}}) \right. \\ &\quad \left. + \frac{|\tilde{\Gamma}_{\mathbf{k}', \mathbf{k}-\mathbf{k}'}^{\beta^\dagger \beta^\dagger} \cdot \mathbf{e}_{\mathbf{k}\lambda}|^2}{2M} \delta(\omega - E_{\mathbf{k}'} - E_{\mathbf{k}-\mathbf{k}'}) [1 + n(E_{\mathbf{k}'})] [1 + n(E_{\mathbf{k}-\mathbf{k}'})] \right] - (\omega \rightarrow -\omega, \mathbf{k} \rightarrow -\mathbf{k}). \end{aligned} \quad (3.22)$$

The attenuation rate $\gamma_{\mathbf{k}\lambda}$ of a phonon with energy $\omega_{\mathbf{k}\lambda}$ can then be obtained from the imaginary part of the self-energy on resonance:

$$\gamma_{\mathbf{k}\lambda} = -\frac{\text{Im}\Sigma_2^{\text{pho}}(\omega_{\mathbf{k}\lambda} + i0, \mathbf{k}, \lambda)}{2\omega_{\mathbf{k}\lambda}}. \quad (3.23)$$

At zero temperature we obtain from Eq. (3.22),

$$\begin{aligned} \gamma_{\mathbf{k}\lambda} &= \frac{\pi}{2\omega_{\mathbf{k}\lambda}} \frac{1}{N} \sum_{\mathbf{k}'} \frac{|\tilde{\Gamma}_{\mathbf{k}', \mathbf{k}-\mathbf{k}'}^{\beta^\dagger \beta^\dagger} \cdot \mathbf{e}_{\mathbf{k}\lambda}|^2}{2M} \\ &\quad \times \delta(\omega_{\mathbf{k}\lambda} - E_{\mathbf{k}'} - E_{\mathbf{k}-\mathbf{k}'}). \end{aligned} \quad (3.24)$$

The leading behavior of $\gamma_{\mathbf{k}\lambda}$ for small \mathbf{k} can be obtained analytically. In this limit it is sufficient to use the linear approximation (2.52) for the magnon dispersion. Moreover, the interaction vertex $\tilde{\Gamma}_{\mathbf{k}, \mathbf{k}'}^{\beta^\dagger \beta^\dagger}$ can be approximated by the leading long-wavelength limit given in Eq. (2.110). The resulting integration can then be carried out analytically and we obtain

$$\gamma_{\mathbf{k}\lambda} = \frac{\pi^2}{64} \left(\frac{\mathbf{k}^2}{2M} \right) \left(\frac{S^2 c_\lambda^2 \mathbf{k}^2}{V_{\text{BZ}} v_x v_y} \right) \frac{I_\lambda(\hat{\mathbf{k}})}{\sqrt{1 - r_{\mathbf{k}\lambda}^2}}, \quad (3.25)$$

where $r_{\mathbf{k}\lambda} = v(\hat{\mathbf{k}})/c_\lambda$, and the dimensionless function $I_\lambda(\hat{\mathbf{k}})$ is given by

$$\begin{aligned}
I_\lambda(\hat{\mathbf{k}}) = & \left(\frac{2s_\theta^2}{c_\theta^2} + 1 \right)^2 \left(1 - r_{\mathbf{k}\lambda}^2 + \frac{3}{8}r_{\mathbf{k}\lambda}^4 \right) \left[\mathbf{f}_1^{X\beta}(\hat{\mathbf{k}}) \cdot \mathbf{e}_{\mathbf{k}\lambda} \right]^2 \\
& + 4s_\theta \frac{v(\hat{\mathbf{k}})}{c_\lambda} \left(\frac{2s_\theta^2}{c_\theta^2} + 1 \right) \left(1 - \frac{3}{4}r_{\mathbf{k}\lambda}^2 \right) \left[\mathbf{f}_1^{X\beta}(\hat{\mathbf{k}}) \cdot \mathbf{e}_{\mathbf{k}\lambda} \right] \left[\mathbf{f}_2^{X\beta}(\hat{\mathbf{k}}, \hat{\mathbf{k}}) \cdot \mathbf{e}_{\mathbf{k}\lambda} \right] \\
& + 2 \left(s_\theta \frac{v(\hat{\mathbf{k}})}{c_\lambda} \right)^2 \left\{ 3 \left[\mathbf{f}_2^{X\beta}(\hat{\mathbf{k}}, \hat{\mathbf{k}}) \cdot \mathbf{e}_{\mathbf{k}\lambda} \right]^2 + (1 - r_{\mathbf{k}\lambda}^2) \left[\mathbf{f}_2^{X\beta}(\hat{\mathbf{k}}, \hat{\mathbf{k}}_\perp) \cdot \mathbf{e}_{\mathbf{k}\lambda} \right]^2 \right\}. \tag{3.26}
\end{aligned}$$

The vector $\hat{\mathbf{k}}_\perp$ in the last line is given by $\hat{\mathbf{k}}_\perp = -(v_y/v_x)\hat{k}_y\mathbf{e}_x + (v_x/v_y)\hat{k}_x\mathbf{e}_y$. We conclude that in the regime of small wavevectors considered here, the ultrasonic attenuation rate is proportional to \mathbf{k}^4 , which shows that in the presence of magnon-phonon interactions the phonons remain well-defined quasiparticles. Let us point out that in order to obtain the correct \mathbf{k}^4 -dependence of the ultrasonic attenuation rate, it is crucial to take the renormalization of the one-phonon two-magnon vertices due to magnon-phonon hybridization into account; see Eqs. (2.101a–2.102c). Otherwise one would incorrectly find from Eq. (3.20) that $\gamma_{\mathbf{k}\lambda}$ reduces to a nonzero constant for $\mathbf{k} \rightarrow 0$, implying that, due to the coupling to the magnon system, the phonons would cease to be well-defined quasiparticles. In the appendix, we show that the interaction processes represented by Fig. 5(b), which involve intermediate states with one magnon and one phonon, also lead to the contribution of the order of \mathbf{k}^4 to the ultrasonic attenuation rate. Fortunately, this contribution is negligible in the experimentally relevant regime where the magnon velocities are small compared with the phonon velocities.

IV. COMPARISON WITH EXPERIMENTS

We have measured the longitudinal c_{22} - and c_{33} -modes propagating in the plane of the two-dimensional layered antiferromagnet Cs_2CuCl_4 down to temperatures of about 50 mK. Experiments as a function of magnetic field were performed in the cone state for fields B parallel to the crystallographic a -axis. For the experiments presented here, we used a setup which allows us to perform simultaneously measurements of changes in the ultrasonic velocity $\Delta c/c_0$ and the relative attenuation $\Delta\alpha$ as a function of an external parameter like temperature or magnetic field. We employ a pulse-echo method using a phase-sensitive detection technique.³⁴ Our measurements can be performed in the frequency range of 5–500 MHz. The duration of the ultrasonic echo pulse is between 0.1 and 1 μs , while the repetition rate is chosen such that it matches the available cooling power in the cryostat. It lies between 100 Hz in the sub-kelvin temperature range, and a few kilohertz at higher temperatures. A high-quality single crystal of the compound Cs_2CuCl_4 with the size of

$3.68 \times 3.8 \times 3.65 \text{ mm}^3$ was grown from aqueous solutions by an evaporation technique.³⁵ Two opposite surfaces normal to the crystallographic b -axis and c -axis were polished and a pair of piezoelectric thin-film transducers was glued to these surfaces. These geometries correspond to the longitudinal c_{22} and c_{33} acoustic modes, with the wavevector \mathbf{k} and polarization $\mathbf{e}_{\mathbf{k}\lambda}$ parallel to the crystallographic b - and c -axis, respectively.

To compare the experimental results with our theoretical predictions, we need realistic estimates for the first and second derivatives $\partial J/\partial x$, $\partial J'/\partial r$, $\partial^2 J/\partial x^2$, and $\partial^2 J'/\partial r^2$ of the exchange couplings for Cs_2CuCl_4 . Recall that these derivatives appear in the explicit expressions (2.71) and (2.72a–2.72c) for the vector $\mathbf{J}_{\mathbf{k}}^{(1)}$ and the tensor $\mathbf{J}_{\mathbf{k}}^{(2)}$, which in turn enter our theoretical results for the elastic constants and the ultrasonic attenuation rate. In principle, the spatial dependence of the exchange couplings can be determined using *ab initio* methods,^{36,37} but quantitative *ab initio* results for the derivatives of the exchange couplings of Cs_2CuCl_4 are currently not available. We therefore model the spatial dependence of our two relevant exchange couplings $J(x)$ and $J'(r)$ by the following phenomenological expressions:

$$J(x) = J(b)e^{-\kappa(x-b)/b}, \tag{4.1a}$$

$$J'(r) = J'(d)e^{-\kappa'(r-d)/d}, \tag{4.1b}$$

where b and $d = \sqrt{b^2 + c^2}/2$ are the bond lengths at the equilibrium positions, and the dimensionless quantities κ and κ' give the inverse range of the exchange interaction in units of the corresponding inverse equilibrium range. Since we do not have any *a priori* knowledge about the numerical values of κ and κ' , we determine these parameters by fitting our theoretical predictions for the elastic constants to the experimental results.

According to Eqs. (2.77) and (3.1) the classical contribution $(\Delta c_\lambda)_0$ to the shift in the phonon velocities arising from the motion of the phonons in the classical spin

background is determined by the dimensionless ratio

$$\lim_{|\mathbf{k}| \rightarrow 0} \frac{\Sigma_0^{\text{pho}}(\mathbf{k}, \lambda)}{\omega_{\mathbf{k}\lambda}^2} = -\frac{S^2}{Mc_\lambda^2} \left\{ s_\theta^2 \left[J\kappa^2 + \frac{J'}{2} \kappa'^2 \cos^4 \varphi_0 \right] + c_\theta^2 \left[J\kappa^2 \cos(Q_x b) + \frac{J'}{2} \kappa'^2 \cos^4 \varphi_0 \cos(Q_x b/2) \right] \right\}, \quad (4.2)$$

for longitudinal phonons in the x -direction (c_{22} -mode), and by

$$\lim_{|\mathbf{k}| \rightarrow 0} \frac{\Sigma_0^{\text{pho}}(\mathbf{k}, \lambda)}{\omega_{\mathbf{k}\lambda}^2} = -\frac{S^2}{2Mc_\lambda^2} J' \kappa'^2 \sin^4 \varphi_0 \times [s_\theta^2 + c_\theta^2 \cos(Q_x b/2)], \quad (4.3)$$

for longitudinal phonons in the y -direction (c_{33} -mode), where $J = J(b)$ and $J' = J'(d)$. Moreover, to evaluate the hybridization contribution $(\Delta c_\lambda)_1$ to the velocity shift given in Eq. (3.14) and the ultrasonic attenuation rate given in Eqs. (3.25, 3.26) we need the dimensionless scalar products $\mathbf{f}_1^{X\beta}(\hat{\mathbf{k}}) \cdot \mathbf{e}_{\mathbf{k}\lambda}$ and $\mathbf{f}_2^{X\beta}(\hat{\mathbf{k}}, \hat{\mathbf{k}}) \cdot \mathbf{e}_{\mathbf{k}\lambda}$, where the vector functions $\mathbf{f}_1^{X\beta}(\hat{\mathbf{k}})$ and $\mathbf{f}_2^{X\beta}(\hat{\mathbf{k}}, \hat{\mathbf{k}})$ are defined in Eqs. (3.13a) and (3.13b). To explain the data for the low-temperature measurements of the longitudinal c_{22} and c_{33} phonon modes, we set $\hat{\mathbf{k}} = (\hat{k}_x, \hat{k}_y) = \mathbf{e}_{\mathbf{k}\lambda}$. In this case the relevant scalar products simplify to

$$\mathbf{f}_1^{X\beta}(\hat{\mathbf{k}}) \cdot \hat{\mathbf{k}} = -\frac{2i}{h_c} \left\{ \hat{k}_x^2 [J\kappa(1 - \cos(Q_x b)) + 2J'\kappa' \cos^2 \varphi_0 (1 - \cos(Q_x b/2))] + \hat{k}_y^2 2J'\kappa' \sin^2 \varphi_0 (1 - \cos(Q_x b/2)) \right\}, \quad (4.4)$$

$$\mathbf{f}_2^{X\beta}(\hat{\mathbf{k}}, \hat{\mathbf{k}}) \cdot \hat{\mathbf{k}} = \frac{i}{v(\hat{\mathbf{k}})} \left\{ \hat{k}_x^3 b [J\kappa \sin(Q_x b) + J'\kappa' \sin(Q_x b/2) \cos^2 \varphi] + 3\hat{k}_x \hat{k}_y^2 c J'\kappa' \sin \varphi_0 \cos \varphi_0 \sin(Q_x b/2) \right\}, \quad (4.5)$$

$$\mathbf{f}_2^{X\beta}(\hat{\mathbf{k}}, \hat{\mathbf{k}}_\perp) \cdot \hat{\mathbf{k}} = \frac{i\hat{k}_x}{v(\hat{\mathbf{k}})} \left\{ \frac{v_y}{v_x} \hat{k}_y^2 b [J\kappa \sin(Q_x b) + J'\kappa' \cos^2 \varphi_0 \sin(Q_x b/2)] + \left[\frac{v_y}{v_x} \hat{k}_y^2 - \frac{v_x}{v_y} \hat{k}_x (\hat{k}_x + \hat{k}_y) \right] \times c J'\kappa' \sin \varphi_0 \cos \varphi_0 \sin(Q_x b/2) \right\}, \quad (4.6)$$

where we have used the fact that the wavevector \mathbf{Q} of the spiral has only an x -component.

Setting $\hat{\mathbf{k}} = (1, 0)$ for the c_{22} -mode and $\hat{\mathbf{k}} = (0, 1)$ for the c_{33} -mode, we can explicitly evaluate the terms in Eq. (3.15) and calculate the velocity shifts. In Fig. 6 we compare our theoretical results for the magnetic-field dependence of the velocity shifts of the longitudinal phonon modes with our experimental data at low temperature.

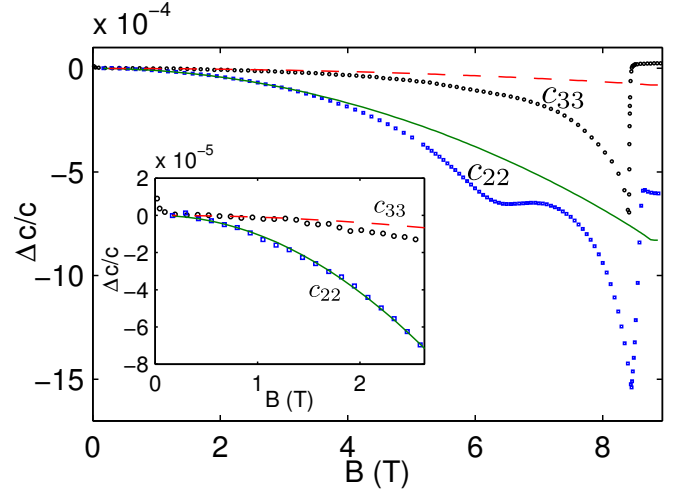


FIG. 6. (Color online) Measured velocity shifts of the longitudinal c_{22} -phonon mode (squares) and the c_{33} -mode (circles) of Cs_2CuCl_4 as a function of the magnetic induction B taken at $T = 52$ mK (c_{22} -mode) and $T = 48$ mK (c_{33} -mode). The solid line is a fit of the data for the c_{22} -mode to our theoretical results at zero temperature given in Eqs. (2.77, 3.1, 3.14, 3.15). From this fit we obtain for our phenomenological parameters κ and κ' introduced in Eqs. (4.1a) and (4.1b) the values $\kappa \approx 15$ and $\kappa' \approx 51$. Using the same values for the c_{33} -mode, we obtain the theoretical prediction represented by the dashed line. From the inset it is obvious that in the weak-field regime $B \lesssim 2.5$ Tesla where our spin-wave approach should be most accurate we obtain excellent agreement between theory and experiment. The anomalies near the critical field $B_c \approx 8.5$ Tesla might have a different physical origin than magnon excitations, so that these features cannot be explained within our spin-wave approach.

The data for the c_{22} -mode was obtained at $T = 52$ mK, while the data for the c_{33} -mode was taken at $T = 48$ mK. The parameters κ and κ' were determined by fitting our theoretical results for the c_{22} -mode to the data. The resulting values $\kappa \approx 15$ and $\kappa' \approx 51$ are then inserted back into our expression for the c_{33} -mode, so that our theoretical prediction for the c_{33} -mode does not contain any adjustable parameters.³⁸ From the inset in Fig. 6 it is obvious that in the weak-field limit $B \lesssim 2.5$ Tesla, where our calculations of the velocity shifts are expected to be most accurate, we obtain excellent agreement between theory and experiment. The deviations between the experimental data and our calculations for larger fields signal the breakdown of our theoretical approach which does not take into account higher order fluctuation corrections and other types of excitations. These are likely to play a role in the vicinity of the critical magnetic field where the magnetic order vanishes. Near the critical field for temperatures below 0.3 K the ultrasonic attenuation exhibits a double peak structure which will be discussed in a separate publication.

Having fixed the fit parameters κ and κ' from the velocity shifts, our theoretical result for the ultrasonic attenuation rate given in Eqs. (3.25) and (3.26) does not

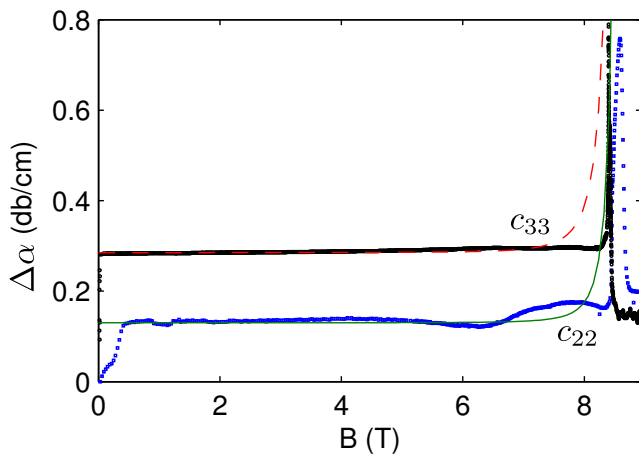


FIG. 7. (Color online) Experimental results for the relative ultrasonic attenuation $\Delta\alpha$ in Cs_2CuCl_4 of the longitudinal c_{22} -phonon mode (squares) and the c_{33} -mode (circles) taken at $T = 52$ mK (c_{22} -mode) and $T = 48$ mK (c_{33} -mode). The solid and the dashed lines represent our corresponding theoretical predictions given in Eqs. (3.25) and (3.26). The attenuation rates have been obtained using the same values $\kappa = 15$ and $\kappa' = 51$ for the fit parameters as in Fig. 6. The constant offset in the attenuation rates is due to the fact that with our experimental technique we can only measure relative attenuation rates. Note that for very small fields the data approaches $\Delta\alpha = 0$.

contain any adjustable parameters. In Fig. 7 we compare the results of our calculations for the attenuation rate of the c_{22} and c_{33} phonon modes with the experimental data of the relative attenuation $\Delta\alpha$. For fields in the range $h \lesssim 0.8h_c$ the measured attenuation rates are rather small, while one observes a strong enhancement for $h \rightarrow h_c$. This indicates that, at least for small magnetic fields, other effects leading to the large attenuation background are not field dependent. The overall shape of the data is reproduced by our theoretical curves rather well, although our spin-wave calculation cannot reproduce the shoulder just below the critical field. Note that according to Eqs. (3.25) and (3.26) the attenuation rate for fields in the vicinity of the critical field can be approximated by

$$\gamma_{\mathbf{k}\lambda} \approx \frac{\pi^2}{64} \left(\frac{\mathbf{k}^2}{2M} \right) \left(\frac{S^2 c_\lambda^2 \mathbf{k}^2}{V_{\text{BZ}} v_x v_y} \right) \frac{[\mathbf{f}_1^{X\beta}(\hat{\mathbf{k}}) \cdot \mathbf{e}_{\mathbf{k}\lambda}]^2}{(1 - h/h_c)^2}, \quad (4.7)$$

where we have approximated $\sin\theta \approx 1$ and $\cos\theta \approx \sqrt{2(1 - h/h_c)}$ for h close to h_c , and have used the fact that in Cs_2CuCl_4 the ratio $r_{\mathbf{k}\lambda} = v(\hat{\mathbf{k}})/c_\lambda$ is small compared with unity. One should keep in mind, however, that in the vicinity of h_c higher order fluctuation corrections which we have neglected within our spin-wave expansions are likely to become important, so that we do not expect that Eq. (4.7) is quantitatively accurate very close to h_c . Nevertheless, from Fig. 7 it is clear that the factor of $(1 - h/h_c)^{-2}$ in Eq. (4.7) gives a satisfactory

description of the strong enhancement of the attenuation rate in the vicinity of the critical field.

V. SUMMARY AND CONCLUSIONS

In summary, we have presented both theoretical and experimental results for the magnetic-field dependence of the elastic constants and the ultrasonic attenuation rate in the cone state of the frustrated quantum antiferromagnet Cs_2CuCl_4 . Our calculations are based on the assumption that two-dimensional magnons are well defined excitations in this material, so that we may use the $1/S$ spin-wave expansion in combination with an expansion in powers of phonon operators. Using a simple phenomenological parametrization of the spatial variations of the exchange couplings involving two adjustable parameters, our theoretical results for the magnetic-field dependence of the elastic constants agree quite well with our experimental measurements, in particular in the weak-field regime $B \lesssim 2.5$ Tesla where our perturbative approach is expected to be most accurate. Our theoretical results for the ultrasonic attenuation rate reproduce the strong enhancement close to the critical magnetic field, although our approach is likely to break down in the vicinity of the quantum critical point.

The fact that the ultrasonic attenuation rate is proportional to \mathbf{k}^4 implies that the coupling to the magnon excitations does not destroy the quasiparticle character of the long-wavelength acoustic phonons. To arrive at this result, it was essential to work out the relevant magnon-phonon matrix elements with great care, taking into account that due to magnon-phonon hybridization in the cone state the cubic part the pure magnon Hamiltonian indirectly contributes to the effective one-phonon two-magnon interaction. Up to now the predicted \mathbf{k}^4 -dependence of the attenuation rate on the phonon momentum could not be detected experimentally. A possible reason is that the magnetic contribution is small compared with the background, which does not depend on the magnetic field. In the vicinity of the critical field, the magnetic contribution becomes large, but it is questionable whether our calculation is still valid in this regime.

We have intentionally restricted the calculations presented in this paper to the magnetically ordered cone state of Cs_2CuCl_4 , because in this case our spin-wave approach is well justified. The investigation of magnon-phonon interactions in the immediate vicinity of the quantum critical point and in the other phases of Cs_2CuCl_4 such as the spin-liquid phase or the ferromagnetic phase is left for future work. Since magnons in frustrated magnets can have anomalous properties such as strong damping,^{39,40} due to magnon-magnon interactions, it should be interesting to take a closer look at these interaction processes between magnons in the cone state, especially in the vicinity of the quantum critical point.

ACKNOWLEDGMENTS

We thank K. Foyevtsova, M. Malard, and R. Valentí for discussions. This work was financially supported by the DFG via SFB/TRR 49 and by the DAAD via the PROBRAL program.

APPENDIX: PROCESSES INVOLVING ONE PHONON AND ONE MAGNON IN THE INTERMEDIATE STATE

In this appendix, we show that in Cs_2CuCl_4 where the phonon velocities are large compared with the magnon velocities the ultrasonic attenuation rate due to processes involving one phonon and one magnon in the intermediate state shown in Fig. 5(b) is small compared with the contribution from processes with two magnons in the intermediate state shown in Fig. 5(a).

Consider the part $H_{1\text{mag}}^{2\text{pho}}$ of the magnon-phonon interaction involving two powers of the phonon operators and one power of the magnon operators. It can be obtained from $H_{\text{spin}}^{\text{npcho}}$ given in Eq. (2.60) by setting $n = 2$ and expanding the spin operators to first order in the Holstein-Primakoff magnon operators. The Fourier transform of the relevant phonon part $U_{\mathbf{k},\mathbf{k}'}^{(2)}$ is given in Eq. (2.66). We obtain

$$H_{1\text{mag}}^{2\text{pho}} = \frac{1}{2!\sqrt{N}} \sum_{\mathbf{k},\mathbf{k}'} \sum_{\lambda\lambda'} \left[\Gamma_{\mathbf{k}\lambda,\mathbf{k}'\lambda'}^{XXb^\dagger} X_{\mathbf{k}\lambda} X_{\mathbf{k}'\lambda'} b_{\mathbf{k}+\mathbf{k}'}^\dagger + \Gamma_{\mathbf{k}\lambda,\mathbf{k}'\lambda'}^{XXb} X_{-\mathbf{k}\lambda} X_{-\mathbf{k}'\lambda'} b_{\mathbf{k}+\mathbf{k}'} \right], \quad (\text{A.1})$$

where the vertices are

$$\Gamma_{\mathbf{k}\lambda,\mathbf{k}'\lambda'}^{XXb^\dagger} = e_{\mathbf{k}\lambda}^\dagger \Gamma_{\mathbf{k}\mathbf{k}'}^{XXb^\dagger} e_{\mathbf{k}'\lambda'}, \quad (\text{A.2})$$

$$\Gamma_{\mathbf{k}\lambda,\mathbf{k}'\lambda'}^{XXb} = e_{\mathbf{k}\lambda}^\dagger \Gamma_{\mathbf{k}\mathbf{k}'}^{XXb} e_{\mathbf{k}'\lambda'}, \quad (\text{A.3})$$

with $\Gamma_{\mathbf{k}\mathbf{k}'}^{XXb^\dagger}$ and $\Gamma_{\mathbf{k}\mathbf{k}'}^{XXb}$ given by the following matrices in the direction labels,

$$\begin{aligned} \Gamma_{\mathbf{k}\mathbf{k}'}^{XXb^\dagger} &= \frac{i}{4} (2S)^{3/2} c_\theta \left[\mathbf{J}_{\mathbf{k}+\mathbf{k}',\mathbf{Q}}^{(2-)} - \mathbf{J}_{\mathbf{k},\mathbf{Q}}^{(2-)} - \mathbf{J}_{\mathbf{k}',\mathbf{Q}}^{(2-)} \right. \\ &\quad \left. - s_\theta (\mathbf{J}_{\mathbf{k}+\mathbf{k}',\mathbf{Q}}^{(2+)} - \mathbf{J}_{\mathbf{k},\mathbf{Q}}^{(2+)} - \mathbf{J}_{\mathbf{k}',\mathbf{Q}}^{(2+)} + \mathbf{J}_{0,\mathbf{Q}}^{(2+)}) \right] \\ &= -\Gamma_{\mathbf{k}\mathbf{k}'}^{XXb}, \end{aligned} \quad (\text{A.4})$$

where the tensors $\mathbf{J}_{\mathbf{k},\mathbf{Q}}^{(2\pm)}$ were introduced in Eqs. (2.78b, 2.78a). From the symmetries in Eq. (2.79) it follows that for small \mathbf{k} and \mathbf{k}' the vertices $\Gamma_{\mathbf{k}\mathbf{k}'}^{XXb^\dagger}$ and $\Gamma_{\mathbf{k}\mathbf{k}'}^{XXb}$ vanish quadratically in \mathbf{k} and \mathbf{k}' . Transforming to the Bogoliubov basis, our Hamiltonian (A.1) assumes the form

$$H_{1\text{mag}}^{2\text{pho}} = \frac{1}{2!\sqrt{N}} \sum_{\mathbf{k},\mathbf{k}'} \sum_{\lambda\lambda'} \left[\Gamma_{\mathbf{k}\lambda,\mathbf{k}'\lambda'}^{XX\bar{b}} X_{\mathbf{k}\lambda} X_{\mathbf{k}'\lambda'} \beta_{\mathbf{k}+\mathbf{k}'}^\dagger + \Gamma_{\mathbf{k}\lambda,\mathbf{k}'\lambda'}^{XX\beta} X_{-\mathbf{k}\lambda} X_{-\mathbf{k}'\lambda'} \beta_{\mathbf{k}+\mathbf{k}'} \right], \quad (\text{A.5})$$

with

$$\Gamma_{\mathbf{k}\mathbf{k}'}^{XX\bar{b}} = u_{\mathbf{k}+\mathbf{k}'} \Gamma_{\mathbf{k}\mathbf{k}'}^{XX\bar{b}} - v_{\mathbf{k}+\mathbf{k}'} \Gamma_{-\mathbf{k},-\mathbf{k}'}^{XXb}, \quad (\text{A.6})$$

$$\Gamma_{\mathbf{k}\mathbf{k}'}^{XX\beta} = u_{\mathbf{k}+\mathbf{k}'} \Gamma_{\mathbf{k}\mathbf{k}'}^{XX\beta} - v_{\mathbf{k}+\mathbf{k}'} \Gamma_{-\mathbf{k},-\mathbf{k}'}^{XX\bar{b}}. \quad (\text{A.7})$$

To second order in the two-phonon one-magnon vertex, we obtain for the phonon self-energy

$$\begin{aligned} \Sigma_3^{\text{pho}}(K, \lambda) &= \frac{T}{N} \sum_{K'\lambda'} \frac{|\Gamma_{\mathbf{k}\lambda,\mathbf{k}'\lambda'}^{XX\beta}|^2}{M^2} G^{\text{pho}}(K'\lambda') G_{\text{mag}}(K'+K) \\ &\quad + (K \rightarrow -K), \end{aligned} \quad (\text{A.8})$$

where $\Gamma_{\mathbf{k}\lambda,\mathbf{k}'\lambda'}^{XX\beta} = e_{\mathbf{k}\lambda}^\dagger \Gamma_{\mathbf{k}\mathbf{k}'}^{XX\beta} e_{\mathbf{k}'\lambda'}$. The Matsubara sums can now be carried, out and we obtain

$$\begin{aligned} \Sigma_3^{\text{pho}}(K, \lambda) &= \frac{1}{N} \sum_{\mathbf{k}'\lambda'} \frac{|\Gamma_{\mathbf{k}\lambda,-\mathbf{k}'\lambda'}^{XX\beta}|^2}{2\omega_{\mathbf{k}'\lambda'} M^2} \left[\frac{n(\omega_{\mathbf{k}'\lambda'}) - n(E_{\mathbf{k}-\mathbf{k}'})}{i\omega + \omega_{\mathbf{k}'\lambda'} - E_{\mathbf{k}-\mathbf{k}'}} \right. \\ &\quad \left. + \frac{n(\omega_{\mathbf{k}'\lambda'}) + n(E_{\mathbf{k}-\mathbf{k}'}) + 1}{i\omega - \omega_{\mathbf{k}'\lambda'} - E_{\mathbf{k}-\mathbf{k}'}} \right] + (K \rightarrow -K), \end{aligned} \quad (\text{A.9})$$

At zero temperature this yields for the ultrasonic attenuation rate

$$\gamma_{\mathbf{k}\lambda} = \frac{\pi}{2\omega_{\mathbf{k}\lambda}} \frac{1}{N} \sum_{\mathbf{k}'\lambda'} \frac{|\Gamma_{\mathbf{k}\lambda,-\mathbf{k}'\lambda'}^{XX\beta}|^2}{2\omega_{\mathbf{k}'\lambda'} M^2} \delta(\omega_{\mathbf{k}\lambda} - \omega_{\mathbf{k}'\lambda'} - E_{\mathbf{k}-\mathbf{k}'}). \quad (\text{A.10})$$

In the long-wavelength limit we obtain for the relevant matrix element of the interaction vertex

$$\begin{aligned} \Gamma_{\mathbf{k},-\mathbf{k}'}^{XX\beta} &= -\frac{i}{4} (2S)^{3/2} \left\{ \right. \\ &\quad s_\theta \sqrt{\frac{\epsilon_{\mathbf{k}-\mathbf{k}'}}{h_c}} (\mathbf{k} \cdot \nabla_{\mathbf{Q}}) (\mathbf{k}' \cdot \nabla_{\mathbf{Q}}) \left[\mathbf{J}_{\mathbf{Q}}^{(2)} \Big|_{\mathbf{Q}=0} - \mathbf{J}_{\mathbf{Q}}^{(2)} \right] \\ &\quad \left. - \frac{c_\theta^2}{2} \sqrt{\frac{h_c}{\epsilon_{\mathbf{k}-\mathbf{k}'}}} [(\mathbf{k} - \mathbf{k}') \cdot \nabla_{\mathbf{Q}}] (\mathbf{k} \cdot \nabla_{\mathbf{Q}}) (\mathbf{k}' \cdot \nabla_{\mathbf{Q}}) \mathbf{J}_{\mathbf{Q}}^{(2)} \right\}. \end{aligned} \quad (\text{A.11})$$

To carry out the integration in Eq. (A.10), we use the fact that in the experimentally relevant regime the phonon velocities are much larger than the magnon velocities. Then the scattering surface defined by $\omega_{\mathbf{k}\lambda} - \omega_{\mathbf{k}'\lambda'} - E_{\mathbf{k}-\mathbf{k}'} = 0$ can be explicitly calculated to leading order in $v(\hat{\mathbf{k}})/c_\lambda$. Using circular coordinates we obtain the parametric representation

$$\mathbf{k}'(\varphi') = |\mathbf{k}| \frac{c_\lambda - u(\hat{\mathbf{k}}, \varphi')}{c_{\lambda'}} \hat{\mathbf{k}}'(\varphi'), \quad (\text{A.12})$$

where $\hat{\mathbf{k}}'(\varphi') = \cos \varphi' \mathbf{e}_x + \sin \varphi' \mathbf{e}_y$, and

$$u(\hat{\mathbf{k}}, \varphi') = \sqrt{v_x^2 (\hat{k}_x - \cos \varphi')^2 + v_y^2 (\hat{k}_y - \sin \varphi')^2}. \quad (\text{A.13})$$

To leading order in $v(\hat{\mathbf{k}})/c_\lambda$ we obtain

$$\gamma_{\mathbf{k}\lambda} = \frac{\pi S^3}{4} \left(\frac{\mathbf{k}^2}{2M} \right) \left(\frac{\mathbf{k}^2}{V_{\text{BZ}}} \right) \sum_{\lambda'} \left(\frac{h_c}{M c_{\lambda'}^2} \right) \left(\frac{c_\lambda}{c_{\lambda'}} \right)^2 \int_0^{2\pi} d\varphi' \frac{u(\hat{\mathbf{k}}, \varphi')}{c_{\lambda'}} |e_{\mathbf{k}\lambda}^\dagger \mathbf{F}^{XX\beta}(\hat{\mathbf{k}}, \varphi') e_{\mathbf{k}'\lambda'}|^2, \quad (\text{A.14})$$

where the dimensionless matrix element is given by

$$\begin{aligned} \mathbf{F}^{XX\beta}(\hat{\mathbf{k}}, \varphi') &= \frac{s_\theta}{h_c} (\hat{\mathbf{k}} \cdot \nabla_{\mathbf{Q}}) (\hat{\mathbf{k}}'(\varphi') \cdot \nabla_{\mathbf{Q}}) \left[\mathbf{J}_{\mathbf{Q}}^{(2)} \Big|_{\mathbf{Q}=0} - \mathbf{J}_{\mathbf{Q}}^{(2)} \right] \\ &\quad - \frac{c_\theta^2}{2u(\hat{\mathbf{k}}, \varphi')} \left[(\hat{\mathbf{k}} - \frac{c_\lambda}{c_{\lambda'}} \hat{\mathbf{k}}'(\varphi')) \cdot \nabla_{\mathbf{Q}} \right] (\hat{\mathbf{k}} \cdot \nabla_{\mathbf{Q}}) (\hat{\mathbf{k}}'(\varphi') \cdot \nabla_{\mathbf{Q}}) \mathbf{J}_{\mathbf{Q}}^{(2)}. \end{aligned} \quad (\text{A.15})$$

Comparing Eq. (A.14) with the corresponding damping rate (3.25) due to one-phonon two-magnon processes, we see that in the experimentally relevant regime where the magnon velocities are small compared with the phonon

velocities, the processes with two magnons in the intermediate states are dominant, although both processes yield contributions to the ultrasonic attenuation rate which are proportional to \mathbf{k}^4 at long wavelengths.

-
- ¹ For a collection of recent reviews see, for example, C. Lacroix, P. Mendels, and F. Mila, *Introduction to Frustrated Magnetism*, Springer Series in Solid-State Sciences 164 (Springer, Berlin, 2011).
- ² A. N. Nasyrov, H. Shodiev, Z. Tylczynski, A. D. Karaev, and V. S. Kim, *Ferroelectrics* **158**, 93 (1994).
- ³ R. Coldea, D. A. Tennant, R. A. Cowley, D. F. McMorrow, B. Dorner, and Z. Tylczynski, *J. Phys.: Condens. Matter* **8**, 7473 (1996).
- ⁴ R. Coldea, D. A. Tennant, R. A. Cowley, D. F. McMorrow, B. Dorner, and Z. Tylczynski, *Phys. Rev. Lett.* **79**, 151 (1997).
- ⁵ S. Bailleul, J. Hölsä, and P. Porcher, *Eur. J. Solid State Inorg. Chem.* **31**, 431 (1994).
- ⁶ R. Coldea, D. A. Tennant, K. Habicht, P. Smeibidl, C. Wolters, and Z. Tylczynski, *Phys. Rev. Lett.* **88**, 137203 (2002).
- ⁷ T. Radu, H. Wilhelm, V. Yushankhai, D. Kovrizhin, R. Coldea, Z. Tylczynski, T. Lühmann, and F. Steglich, *Phys. Rev. Lett.* **95**, 127202 (2005).
- ⁸ M. Y. Veillette, J. T. Chalker, and R. Coldea, *Phys. Rev. B* **71**, 214426 (2005).
- ⁹ M. Y. Veillette, A. J. A. James, and F. H. L. Essler, *Phys. Rev. B* **72**, 134429 (2005).
- ¹⁰ M. Y. Veillette and J. T. Chalker, *Phys. Rev. B* **74**, 052402 (2006).
- ¹¹ D. Dalidovich, R. Sknepnek, A. J. Berlinsky, J. Zhang, and C. Kallin, *Phys. Rev. B* **73**, 184403 (2006).
- ¹² D. L. Kovrizhin, V. Yushankhai, and L. Siurakshina, *Phys. Rev. B* **74**, 134417 (2006).
- ¹³ M. Q. Weng, D. N. Sheng, Z. Y. Weng, and R. J. Bursill, *Phys. Rev. B* **74**, 012407 (2006).
- ¹⁴ M. Kohno, O. A. Starykh, and L. Balents, *Nat. Phys.* **3**, 790 (2007).
- ¹⁵ O. A. Starykh and L. Balents, *Phys. Rev. Lett.* **98**, 077205 (2007).
- ¹⁶ M. Kohno, *Phys. Rev. Lett.* **103**, 197203 (2009).
- ¹⁷ O. A. Starykh, H. Katsura, and L. Balents, *Phys. Rev. B* **82**, 014421 (2010).
- ¹⁸ C. H. Chung, J. B. Marston, and R. H. McKenzie, *J. Phys.: Condens. Matter* **13**, 5159 (2001).
- ¹⁹ J. O. Fjærestad, W. Zheng, R. R. P. Singh, R. H. McKenzie, and R. Coldea, *Phys. Rev. B* **75**, 174447 (2007).
- ²⁰ B. Lüthi, *Physical Acoustics in the Solid State* (Springer, Berlin, 2005).
- ²¹ A. Sytcheva, O. Chiatti, J. Wosnitza, S. Zherlitsyn, A. A. Zvyagin, R. Coldea, and Z. Tylczynski, *Phys. Rev. B* **80**, 224414 (2009).
- ²² M. Tachiki and S. Maekawa, *Prog. Theor. Phys.* **51**, 1 (1974).
- ²³ A. R. Lim and J. K. Jung, *Solid State Commun.* **132**, 393 (2004).
- ²⁴ S. Aplešnin, *Phys. Lett. A* **333**, 446 (2004).
- ²⁵ J. H. Kim and J. H. Han, *Phys. Rev. B* **76**, 054431 (2007).
- ²⁶ Y. Zhou and P. A. Lee, *Phys. Rev. Lett.* **106**, 056402 (2011).
- ²⁷ R. Coldea, D. A. Tennant, and Z. Tylczynski, *Phys. Rev. B* **68**, 134424 (2003).
- ²⁸ F. Schütz, M. Kollar, and P. Kopietz, *Phys. Rev. Lett.* **91**, 017205 (2003).
- ²⁹ I. Spremo, F. Schütz, P. Kopietz, V. Pashchenko, B. Wolf, M. Lang, J. W. Bats, C. Hu, and M. U. Schmidt, *Phys. Rev. B* **72**, 174429 (2005).
- ³⁰ K. Foyevtsova (private communication).
- ³¹ N. Hasselmann and P. Kopietz, *Europhys. Lett.* **74**, 1067 (2006).
- ³² A. Kreisel, F. Sauli, N. Hasselmann, and P. Kopietz, *Phys. Rev. B* **78**, 035127 (2008).
- ³³ A. Perelomov, *Generalized Coherent States and Their Applications* (Springer, Berlin, 1986).
- ³⁴ B. Lüthi, G. Bruls, P. Thalmeier, B. Wolf, D. Finsterbusch, and I. Kouroudis, *J. Low Temp. Phys.* **95**, 257 (1994).
- ³⁵ N. Krüger, S. Belz, F. Schossau, A. A. Haghighirad, P. T. Cong, B. Wolf, S. Gottlieb-Schoenmeyer, F. Ritter, and W. Assmus, *Cryst. Growth Des.* **10**, 4456 (2010).
- ³⁶ Y.-Z. Zhang, H. O. Jeschke, and R. Valentí, *Phys. Rev. B* **78**, 205104 (2008).
- ³⁷ K. Foyevtsova, I. Opahle, Y. Zhang, H. O. Jeschke, and

R. Valentí, Phys. Rev. B **83**, 125126 (2011).

- ³⁸ Note that the c_{33} -phonons do not modulate the bond lengths of the coupling J , so that the associated velocity shift depends only on κ' .

³⁹ A. L. Chernyshev and M. E. Zhitomirsky, Phys. Rev. Lett. **97**, 207202 (2006).

⁴⁰ A. L. Chernyshev and M. E. Zhitomirsky, Phys. Rev. B **79**, 144416 (2009).